Geophysical Journal International

Geophys. J. Int. (2018) **212,** 1546–1569
Advance Access publication 2017 November 3
GJI Seismology

doi: 10.1093/gji/ggx479

Crust and uppermost-mantle structure of Greenland and the Northwest Atlantic from Rayleigh wave group velocity tomography

Fiona A. Darbyshire,[1] Trine Dahl-Jensen,[2] Tine B. Larsen,[2] Peter H. Voss[2] and Guillaume Joyal[1]

[1]*Centre de recherche GEOTOP, Université du Québec à Montréal, CP* 8888 *succursale Centre-Ville, Montréal, QC* H3C 3P8*, Canada.*
E-mail: darbyshire.fiona_ann@uqam.ca
[2]*Geological Survey of Denmark and Greenland, Oster Voldgade* 10, DK-1350 *Copenhagen K, Denmark*

Accepted 2017 November 2. Received 2017 October 31; in original form 2017 September 1

SUMMARY

The Greenland landmass preserves ∼4 billion years of tectonic history, but much of the continent is inaccessible to geological study due to the extensive inland ice cap. We map out, for the first time, the 3-D crustal structure of Greenland and the NW Atlantic ocean, using Rayleigh wave anisotropic group velocity tomography, in the period range 10–80 s, from regional earthquakes and the ongoing GLATIS/GLISN seismograph networks. 1-D inversion gives a pseudo-3-D model of shear wave velocity structure to depths of ∼100 km with a horizontal resolution of ∼200 km. Crustal thickness across mainland Greenland ranges from ∼25 km to over 50 km, and the velocity structure shows considerable heterogeneity. The large sedimentary basins on the continental shelf are clearly visible as low velocities in the upper ∼5–15 km. Within the upper continental basement, velocities are systematically lower in northern Greenland than in the south, and exhibit a broadly NW–SE trend. The thinning of the crust at the continental margins is also clearly imaged. Upper-mantle velocities show a clear distinction between typical fast cratonic lithosphere ($Vs \geq 4.6\,km\,s^{-1}$) beneath Greenland and its NE margin and anomalously slow oceanic mantle ($Vs \sim 4.3–4.4\,km\,s^{-1}$) beneath the NW Atlantic. We do not observe any sign of pervasive lithospheric modification across Greenland in the regions associated with the presumed Iceland hotspot track, though the average crustal velocity in this region is higher than that of areas to the north and south. Crustal anisotropy beneath Greenland is strong and complex, likely reflecting numerous episodes of tectonic deformation. Beneath the North Atlantic and Baffin Bay, the dominant anisotropy directions are perpendicular to the active and extinct spreading centres. Anisotropy in the subcontinental lithosphere is weaker than that of the crust, but still significant, consistent with cratonic lithosphere worldwide.

Key words: Arctic region; Seismic anisotropy; Seismic tomography; Surface waves and free oscillations; Crustal structure.

1 INTRODUCTION

Greenland and the North Atlantic region have a long and complex tectonic history. Mainland Greenland, originally part of the Laurentian core of North America, is largely underlain by a Precambrian continental shield consisting of an Archean craton and a number of Palaeoproterozoic belts. The continent preserves several Palaeozoic continental collisions, most notably the Caledonian-Appalachian mountain chain arising from the closure of the Iapetus ocean. Rifting from the rest of Laurentia in Cretaceous—Palaeogene times opened the Labrador Sea and Baffin Bay between present-day Greenland and Canada; continental breakup subsequently concentrated east of Greenland, with the opening and continued spreading of the North Atlantic ocean.

With the exception of the Greenland continental margins and parts of the North Atlantic ocean basin, the crustal structure of the region as a whole has not been studied in detail. Point measurements of crustal thickness and bulk composition beneath a sparse network of seismic stations across Greenland have been made, but there has been little to no information available on structural variability within the crust to date.

In this study, we use Rayleigh wave group velocities at periods of 10–80 s, derived from North Atlantic and Arctic regional earthquakes recorded at seismic stations in Greenland and northernmost

Canada, to constrain the velocity structure of the crust and uppermost mantle across Greenland and the NW Atlantic.

1.1 Geology and tectonics

The Greenland landmass comprises over 2 million km^2 of which only 19 per cent is exposed rock; the rest being covered by an extensive inland ice sheet up to at least 3 km thick (Bamber *et al.* 2001; Henriksen *et al.* 2009). Much of Greenland is thought to be underlain by Precambrian basement making up a shield region that stabilized as part of the Laurentian landmass ~1.6 Ga ago (Henriksen *et al.* 2009). During the later Proterozoic and the Phanerozoic, successions of rifting and orogenic events along the margins of the Greenland shield led to the formation of both extensive fold belts and deep sedimentary basins. The geology of the Greenland interior remains largely unknown due to the inland ice; however, efforts have been made to use indirect methods to map out the major geologic provinces beneath the ice cap (e.g. Dawes 2009; St-Onge *et al.* 2009).

Much of southern Greenland is underlain by part of the Archean North Atlantic craton (e.g. van Gool *et al.* 2002; St-Onge *et al.* 2009; Henriksen *et al.* 2009) (NAC; Fig. 1). The craton has been largely unaffected by Proterozoic or later orogenic activity. South of the craton, the Palaeoproterozoic Ketilidian orogenic belt (KMB; Fig. 1), composed largely of juvenile Palaeoproterozoic rocks, underlies the southern tip of the Greenland landmass. To the north, two orogenic belts made up of reworked Archean rocks, were initially identified; the Nagssugtoqidian belt (NMB) in the west and the Ammassalik belt (AMB) in the southeast (Fig. 1). However, magnetic anomaly data (e.g. Verhoef *et al.* 1996) suggest that the eastern outcrops are most likely a continuation of the Nagssugtoqidian orogen. Further north, the exposed basement in western Greenland is dominated by reworked Archean rocks of the Rinkian fold belt (RMB) and juvenile Palaeoproterozoic rocks of the Inglefield orogenic belt (IMB), both thought to be correlated with the Canadian Rae craton and Foxe belt (e.g. van Gool *et al.* 2002; St-Onge *et al.* 2009).

Tectonic structures in northern and eastern Greenland are dominated by Palaeozoic sedimentary basins and major orogenic belts (e.g. Henriksen *et al.* 2009). The Palaeozoic Franklinian basin covers most of northern Greenland, with sedimentation occurring from latest Precambrian until early Devonian times. The late Palaeozoic Ellesmerian orogeny subsequently created an extensive E–W to NE–SW trending fold belt in the north (Fig. 1, Franklinian and Ellesmerian labelled as North Greenland Fold Belt; NGFB). The closure of the Iapetus ocean and Laurentia-Baltica collision in the mid-Silurian created the vast Caledonian-Appalachian orogenic belt (CFB; Fig. 1), of which a ~1300 km length is preserved along an N-S trend in eastern Greenland (e.g. Schmidt-Aursch & Jokat 2005; Henriksen *et al.* 2009). The orogeny was followed by extensional collapse and sedimentary basin development in the Devonian, and a succession of rifting events, culminating in the opening of the North Atlantic from ~56 Ma ago.

Greenland separated from North America by rifting and seafloor spreading between mid-Cretaceous and Oligocene times (e.g. Chalmers & Pulvertaft 2001; Torsvik *et al.* 2002). Central Baffin Bay and the Labrador Sea (BB, LS; Fig. 2) are underlain by oceanic crust, though the Davis Strait (DS; Fig. 2) between the two basins is thought to be underlain by thinned continental crust (Funck *et al.* 2007).

Extensive plateau basalts outcrop in both central-western and central-eastern Greenland, thought to be associated with the initial phases of continental breakup and North Atlantic opening between ~62 and 58 Ma ago. These plateau basalts are part of a wider sequence of magmatic activity across the entire North Atlantic, related to the impingement of the Iceland plume (e.g. Nielsen *et al.* 2002). Volcanic rifted margins are found offshore central-western, southeastern and central-eastern Greenland, characterized by seaward-dipping reflectors and extensive lower-crustal intrusions (e.g. Holbrook *et al.* 2001; Hopper *et al.* 2003). A band of thickened oceanic crust stretches from SE Greenland through Iceland to the Faeroe Islands (e.g. Smallwood *et al.* 1999; Darbyshire *et al.* 2000; Holbrook *et al.* 2001) (GIR—FIR; Fig. 2).

Breakup between Greenland and northern Europe began in the Palaeocene, but the development of seafloor spreading and the opening of the ocean basins from south to north was spread over tens of Ma (e.g. Talwani & Eldholm 1977; Torsvik *et al.* 2002; Engen *et al.* 2008). Opening of the North Atlantic in the Iceland/Jan Mayen (JM; Fig. 2) region was complex, involving a number of ridge jumps (e.g. Torsvik *et al.* 2002; Henriksen *et al.* 2009). Spreading is generally oblique, and sometimes asymmetric, with spreading rates ranging from slow (<55–60 mm yr^{-1} full rate) in the south to ultraslow (<12–20 mm yr^{-1} full rate; Dick *et al.* 2003) in the north.

1.2 Previous seismic studies

Due to the inaccessibility of the Greenland interior, few studies of crustal structure on the mainland were carried out before the beginning of the 21st century. Gregersen (1970) used two-station group and phase velocity measurements to estimate an average crustal model with a Moho depth of 43 km (crustal thickness of 40 km). Other studies of Greenland and its surroundings were restricted to the coast, the continental shelf and margins, and the ocean basins, mostly based on marine active-source seismic studies (e.g. Chian & Louden 1992, 1994; Jackson & Reid 1994; Kodaira *et al.* 1997; Dahl-Jensen *et al.* 1998; Schlindwein & Jokat 1999).

From 1999 to 2003, a new network of seismograph stations was placed across Greenland, both on the ice-free coasts and across the Greenland icecap, through the GLATIS (Greenland Lithosphere Analysed Teleseismically on the Ice Sheet) and NEAT (NE Atlantic Tomography) projects. Using receiver function analysis, Dahl-Jensen *et al.* (2003) made the first detailed measurements of Moho depth variation across Greenland. They found a wide range of crustal thicknesses, from <25 km close to the eastern and northern rift basins to ~50 km in central Greenland. Variations in crustal thickness were interpreted as the signature of two distinct Proterozoic blocks north of the south Greenland Archean craton. The receiver function data set was subsequently reanalysed by Kumar *et al.* (2007), using both Ps and Sp receiver functions. Although their findings were broadly similar to those of Dahl-Jensen *et al.* (2003), they estimated thinner crust (~40–42 km) in central Greenland with no clear division of domains based on Moho depth. Both receiver function studies included forward modelling to take into account the ice layer beneath the inland stations. Receiver functions from a short broad-band transect in east Greenland (Schiffer *et al.* 2014) showed crustal thinning towards the coast, from 41 to 25 km, and suggestions of a fossil subduction zone in the uppermost mantle.

In addition to the Greenland receiver function studies, further information on crustal structure has been gathered from marine active-source experiments. Parts of the Greenland margin have been extensively studied (e.g. Korenaga *et al.* 2000; Holbrook *et al.* 2001; Hopper *et al.* 2003; Schmidt-Aursch & Jokat 2005;

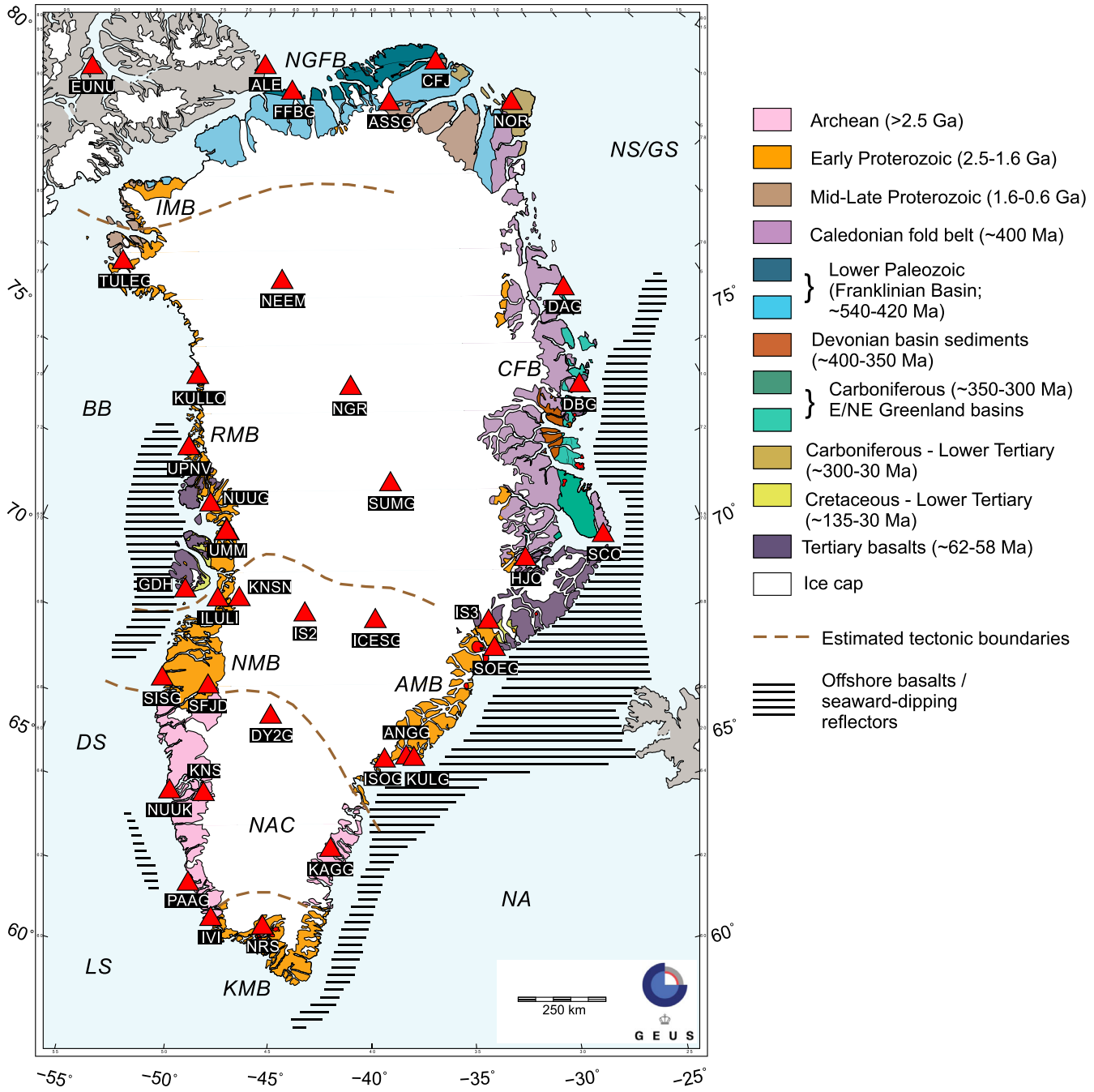

Figure 1. Station locations (red triangles) overlain on simplified Greenland geology, after Henriksen *et al.* (2009). NAC, North Atlantic Craton; IMB, Inglefield Mobile Belt; RMB, Rinkian Mobile Belt; KMB, Ketilidian Mobile Belt; AMB, Ammassalik Mobile Belt; NMB, Nagssugtoqidian Mobile Belt; CFB, Caledonian Fold Belt; NGFB, North Greenland Fold Belt; BB, Baffin Bay; DS, Davis Strait; LS, Labrador Sea; NS/GS, Norwegian-Greenland Sea; NA, North Atlantic Ocean. Dashed brown lines indicate estimated positions of major tectonic boundaries beneath the icecap (St-Onge *et al.* 2009).

Voss & Jokat 2007; Voss *et al.* 2009; Jackson & Dahl-Jensen 2010), and several refraction profiles have constrained crustal structure across the Davis Strait (e.g. Funck *et al.* 2007; Gerlings *et al.* 2009; Suckro *et al.* 2013), Baffin Bay (e.g. Funck *et al.* 2012; Suckro *et al.* 2012) and Nares Strait (e.g. Funck *et al.* 2006). A summary of onshore and marine seismic experiments and resulting Moho depth estimates is shown in the Supporting Information.

Tomographic inversion of group velocities from 15 to 200 s period for the Arctic region as a whole was carried out by Levshin *et al.* (2001), providing information on both isotropic heterogeneity and azimuthal anisotropy. The models include the whole of Greenland, but are smooth in nature, and path density across the Greenland mainland is low compared with many other regions of the model. Greenland is characterized by lower than average group velocities for periods of 40 s and below (periods which sample continental crust and oceanic mantle), whereas the thick cratonic lithosphere shows up as anomalously high group velocities at longer periods. Azimuthal anisotropy is largely ridge-perpendicular in the North Atlantic, rotating to a dominantly ∼NE–SW orientation across most of Greenland.

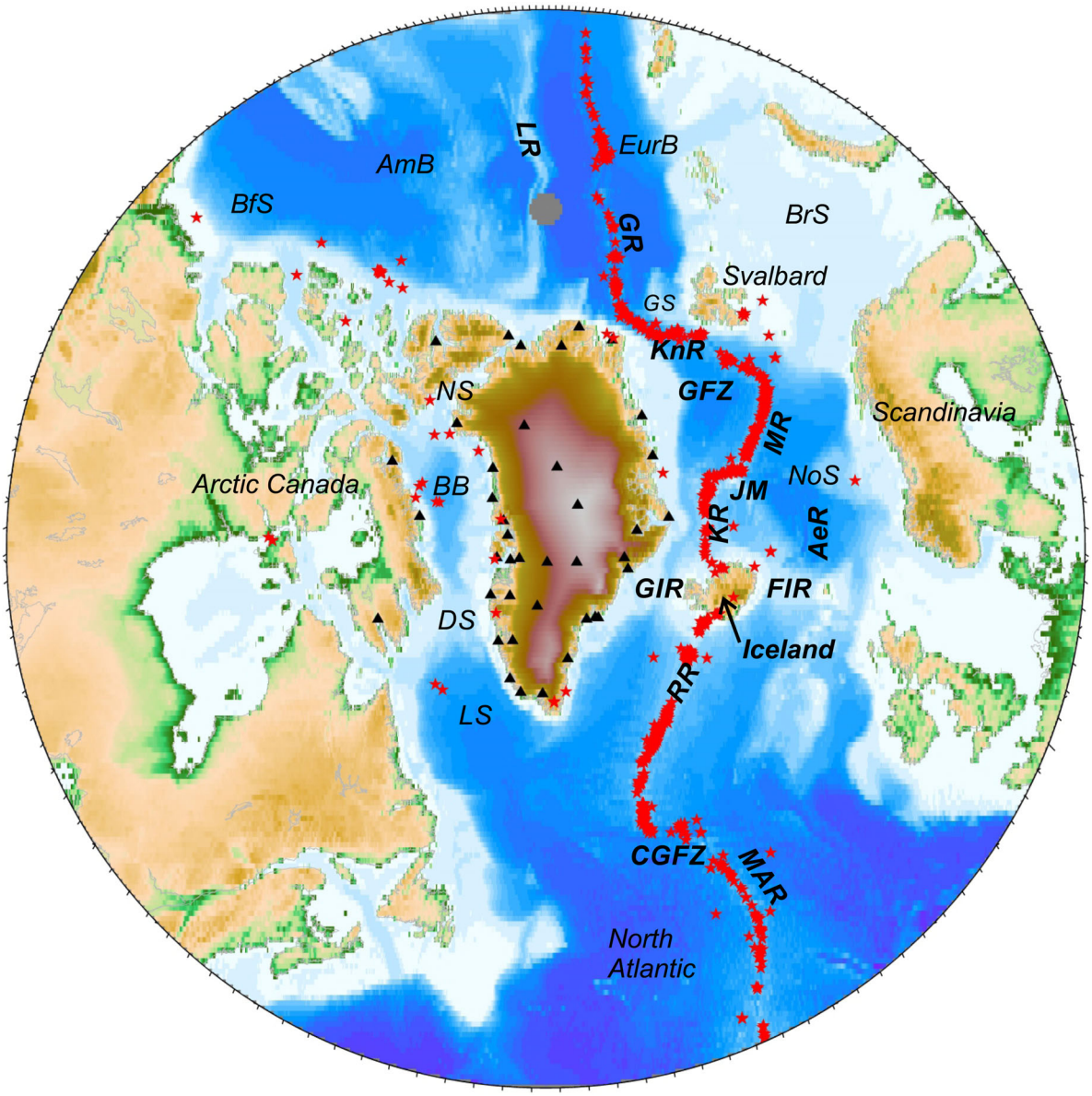

Figure 2. North Atlantic/Arctic region with seismograph stations (black triangles) and earthquakes (red stars) used in the study. The background map shows topography/bathymetry. MAR, Mid-Atlantic Ridge; CGFZ, Charlie Gibbs Fracture Zone; RR, Reykjanes Ridge; GIR, Greenland-Iceland Ridge, FIR, Faeroe-Iceland Ridge; KR, Kolbeinsey Ridge; AeR, Aegir Ridge; JM, Jan Mayen; MR, Mohns Ridge; GFZ, Greenland Fracture Zone; KnR, Knipovich Ridge; GR, Gakkel Ridge; LR, Lomonosov Ridge; LS, Labrador Sea; DS, Davis Strait; BB, Baffin Bay; NS, Nares Strait; BrS, Barents Sea; BfS, Beaufort Sea; EurB, Eurasian Basin; AmB, Amerasian Basin; GS, Greenland Sea; NoS, Norwegian Sea.

Most subsequent seismic images of the Greenland and North Atlantic region as a whole come from either large-scale regional seismic studies (e.g. Pilidou *et al.* 2004; Jakovlev *et al.* 2012; Rickers *et al.* 2013) or from global-scale tomographic models of various smoothness, resolution and depth range (e.g. Ritsema *et al.* 2011; Schaeffer & Lebedev 2013, 2014). The main focus of these models, however, is the mantle structure, dominated by the high velocities of the Greenland cratonic mantle lithosphere and low velocities of the North Atlantic upper mantle; generally crustal depths in these models are either unresolved or at the limits of model resolution. A more recent global/regional tomographic model (Lebedev *et al.* 2017) focusses on the lithospheric structure of the Circum-Arctic region, with results presented for a depth range of 36–330 km. The depth range therefore likely includes the lower crust beneath much of mainland Greenland, as well as the entire mantle lithosphere.

2 SEISMOGRAPH NETWORKS AND REGIONAL DATA SET

Our data set consists of recordings of regional earthquakes at 38 broad-band seismograph stations in Greenland and 5 in the eastern Canadian Arctic (Figs 1 and 2; Table 1), over a time period from early 1999 to autumn 2013. The station operating periods and affiliations vary across the network; some operated for only a few months, while others have been in continuous operation for over a decade. Many of the Greenland stations were initially installed in short-term deployments through the GLATIS (Greenland Lithosphere Analysed Teleseismically on the Ice Sheet) project, with subsequent re-occupation of the sites from 2010 onwards through the multinational GLISN (Greenland Ice Sheet Monitoring Network) project. Other longer-term stations are affiliated to

Table 1. List of seismograph stations used in the study. CN, CNSN: Canadian National Seismograph Network; DK: Danish National Seismograph Network; GE: GEOFON permanent network (GFZ Potsdam); G: Geoscope; GLATIS: Greenland Lithosphere Analysed Teleseismically on the Ice Sheet; GLISN: Greenland Icesheet Monitoring Network; GSN: Global Seismograph Network (IRIS); NEAT: North East Atlantic Tomography; KP: Korea Polar Seismic Network; UAF: U. Alaska Fairbanks. Stations ILULI, KULLO and NUUG are operated by ETH Zurich. Station ICESG is operated by IRIS and JAMSTEC (Japan). 'pr': station presently in operation.

Station Code	Latitude	Longitude	Elev. (m)	Network/Project	Operation
ALE	82.500	−62.350	60	II/GSN,GLISN	1990–pr
ANGG	65.6160	−37.6370	0	DK/GLATIS,NEAT,GLISN	2000–2009,2010–pr
ASIG	68.7060	−52.8710	60	DK	2004–2006
ASSG	82.1762	−38.1082	318	DK	2004–2005
CFJ	83.0835	−28.3208	60	DK	2004–2007
CLRN	70.4743	−68.5871	9	CN/CNSN	2011–pr
DAG	76.7713	−18.6550	23	GE/GLATIS,GLISN	1998–pr
DBG	74.3080	−20.2139	10	DK/GLATIS,NEAT,GLISN	2000–2006,2010–pr
DY2G	66.4740	−46.2639	2110	DK/GLATIS,GLISN	2000,2011–pr
EUNU	80.0532	−86.4158	623	CN/CHASME	2000–pr
FFBG	82.1294	−56.0338	30	DK	2004–2006
FRB	63.7469	−68.5451	25	CN/CNSN	1992–pr
GDH	69.2500	−53.5333	23	DK/GLATIS	2000–2001
HJO	70.3522	−28.1640	40	DK/GLATIS	2000–2002
ICESG	69.0922	−39.6474	2932	DK/GLISN	2011–pr
ILULI	69.2121	−51.1048	53	DK/GLISN	2009–pr
IS2	69.1660	−44.7357	2220	DK/GLATIS	2000
IS3	68.9058	−31.5395	2211	DK/GLATIS	2000
ISOG	65.5480	−38.9754	12	DK/GLISN	2007–2009,2012–pr
IVI	61.2000	−48.1833	20	G/GLISN	2011–pr
KAGG	63.2485	−42.0349	28	DK/GLATIS	2000–2002
KNS	64.290	−49.680	290	9D/UAF	2010–2012
KNSN	64.320	−49.590	400	9D/UAF	2010–2012
KULG	65.5752	−37.1788	50	DK	2004–2006
KULLO	74.5805	−57.2201	44	DK/GLISN	2005,2009–pr
NEEM	77.4447	−51.0738	2513	DK/GLISN	2007–2010,2011–pr
NGR	75.0010	−42.3148	2960	DK/GLATIS	1999–2003
NOR	81.6000	−16.6833	36	DK/GLISN	2002–pr
NRS	61.1595	−45.4188	65	DK/GLATIS,GLISN	2000–2001,2010–pr
NUUG	71.5384	−53.1996	36	DK/GLISN	2010–pr
NUUK	64.1838	−51.6679	110	DK/GLATIS,NEAT,GLISN	2000–2003,2010–pr
PAAG	61.9914	−49.6613	22	DK/GLATIS	2000–2001
PINU	72.6971	−77.9748	36	CN/CHASME	2000–2007
SCO	70.4833	−21.9500	69	DK/GLATIS,GLISN	1999–2001,2010–pr
SFJ	66.9967	−50.6156	365	IU/GLATIS,GLISN	1996–2005
SFJD	66.9960	−50.6215	330	IU/GLATIS,GLISN	2005–pr
SISG	66.9366	−53.6430	0	DK	2006–2007
SOEG	68.2033	−31.3770	1	DK/GLATIS,GLISN	2000–2002,2010–pr
SUMG	72.5763	−38.4539	3240	GE/GLATIS,GLISN	2000–pr
TULEG	76.5374	−68.8238	40	CN/CHASME; DK/GLISN	2000–2009,2010–pr
UMM	70.6774	−52.1249	48	DK	2004–2006
UPNG	72.7850	−56.1410	30	CN/CHASME,GLATIS	1999–2000
UPNV	72.780	−56.140	38	KP/GLISN	2013–pr

the IRIS Global Seismograph Network, the GEOFON permanent global network or the Danish and Canadian national seismograph networks.

Earthquake catalogues were searched for events in the North Atlantic and Arctic regions, with an initial minimum-magnitude cut-off of 4.5. The vast majority of the earthquakes fall along the Mid-Atlantic Ridge; however there were also a few intraplate earthquakes from northern Canada, the Norwegian Sea and the Svalbard region (Fig. 2). For each event, a half-hour data file was requested. In some cases, multiple high-quality arrivals were visible within this window; for each waveform, the catalogues were searched to identify the event and it was added to the data set. Earthquake swarms in the region southwest of Iceland were particularly well-recorded at stations in southeast Greenland, and magnitudes as low as 3.7 gave signals clear enough for analysis.

Following initial quality control and basic data processing, the instrument response was removed from each seismogram, and a zero-phase bandpass filter was applied to suppress microseismic noise and long-period instabilities resulting from the response removal. The typical filter bandwidth was 10–100 s, though some of the noisier sites required a narrower-band filter such as 10–60 s.

3 RAYLEIGH WAVE GROUP VELOCITIES

3.1 Dispersion measurements

Surface wave group velocities from regional earthquakes are well suited to studies of the crust and uppermost mantle, as regional

earthquakes typically contain energy at periods sensitive to crustal depths. While measurement errors are typically larger than those for phase velocities for a given period range, and the sensitivity kernels are somewhat more complex, group velocities remain a valuable analysis tool. Unlike phase velocity measurement, the analysis does not require detailed knowledge of the source-time function of the earthquake. This allows a wider range of earthquakes—particularly smaller events in more remote regions—to be used and therefore improves the source-station path coverage for tomographic inversions. In addition, group velocities have been shown to be more sensitive to the Moho than the corresponding phase velocities (Lebedev *et al.* 2013). Group velocity tomography has been a popular technique for imaging crust and upper-mantle structure for several decades, and is widely used in both ambient-noise and earthquake-based studies.

The group velocity of a Rayleigh wave can be measured by tracking the maximum amplitude of the wave-train envelope as a function of both time and frequency (e.g. Levshin *et al.* 1992). From the frequency–time analysis, if the source-station distance is known, the group velocity as a function of wave period can be calculated. Here we use a multiple-filter analysis technique to extract the frequency-time-amplitude information from the seismograms for each individual source-station path. We use the implementation of Herrmann (2013), which produces a graphical user interface for the frequency–time (in this case, period–group velocity) data from which the user can manually pick the envelope maximum (Fig. 3). Such visual inspection is useful for making well-constrained estimates of group velocity while avoiding instabilities related to noise or spectral holes. Group velocity measurements for each source-station path were typically made over a period range of 10–80 s, though a few events yielded shorter (down to 5 s) or longer (up to 100 s) period data.

For each station, the number of individual source-station group velocity curves varied depending on signal quality at the station, period of operation and seismicity during the period of operation. The longest-operating stations yielded several hundred dispersion curves. In order to reduce path bias and to improve the consistency of the data, we binned sets of earthquakes from similar source regions for a given station, using latitude bins of up to 1° and longitude bins of 1°–3° (where the larger ranges were appropriate at the highest latitudes). Group velocity curves in each bin were plotted individually to check for outliers or unstable results, then averaged to produce a composite group velocity curve for each bin. As with the total number of measurements, the number of successful bins varied with operation time of the station, with up to 70 bins for the longest-running stations. A total of 1202 binned source-station paths was kept for further analysis.

The multiple-filter analysis provides individual measurement errors for each dispersion curve, which vary according to data quality and generally increase with increasing period. The averaging of multiple dispersion curves for the source-station path bins mitigates errors from individual curves but gives rise to a new set of uncertainties for the dispersion measurements, based on the spread of the individual curves in each bin. In order to deal with the final uncertainties in a systematic fashion, we examined the range of error measurements for individual curves, the spread of group velocity values in the binned measurement sets and the range of typical group velocity uncertainties in the literature. Based on this information, we assigned new error bars to the ensemble of final curves, scaled with period, from 0.04 km s^{-1} at 10 s period to 0.11 km s^{-1} at 80 s period.

3.2 Tomographic inversion

Least-squares inversion (Paige & Saunders 1982) was used to combine the source-station paths into group velocity maps for 15 periods between 10 and 80 s, solving simultaneously for isotropic velocity heterogeneity and azimuthal anisotropy. Here we use the method described by Deschamps *et al.* (2008) and Darbyshire & Lebedev (2009), in which the inversion is carried out across a triangular grid of knot points spaced evenly across the region covered by the surface wave paths. This method has been primarily used in studies using 2-station phase velocity data (e.g. Deschamps *et al.* 2008; Darbyshire & Lebedev 2009; Darbyshire *et al.* 2013), but has also been successfully implemented in group velocity studies (e.g. Pawlak *et al.* 2012). The grid spacings used in this study were 100 km for the model grid and 30 km for the integration grid.

At each model grid knot, we invert for five unknowns in group velocity, assuming a weakly anisotropic medium:

$$\delta U(\omega) = \delta U_{\mathrm{iso}}(\omega) + A1(\omega)\cos(2\psi) + B1(\omega)\sin(2\psi) + A2(\omega)\cos(4\psi) + B2(\omega)\sin(4\psi), \quad (1)$$

where δU_{iso} is the isotropic group velocity anomaly, 2ψ is the variation of the group velocity with π periodicity, and 4ψ is the variation with $\pi/2$ periodicity (Smith & Dahlen 1973). The model is governed by a system of linear equations relating the average group velocity along each source-station path, the wave sensitivity area for the path at a point in the model and the group velocity anomaly. The sensitivity areas are approximated by zero-width rays for simplicity. Finite-width rays were also tested, but the results were similar (likely within measurement error) to the zero-width approximation in well-resolved regions, with only the model edges showing significant differences.

The model is regularized via both smoothing and gradient-damping parameters, which penalize the second and first derivatives of the anomaly distribution, respectively. Parameters were chosen based on assessment of trade-off curves between variance reduction and model roughness, as well as visual inspection of the resulting group velocity maps. The anisotropic parameters were smoothed more strongly than the isotropic component since their resolution is generally lower (e.g. Darbyshire & Lebedev 2009; Pawlak *et al.* 2012).

Due to the variable frequency content of both individual group velocity measurement and binned curves, the number of paths used in the inversion varies significantly with wave period (Fig. 4), from a minimum of 169 (80 s period) to a maximum of 1077 (30 s period). Much of Greenland and the western Atlantic region are well covered by crossing ray paths for the entire period range; in contrast, coverage of the Baffin Bay area is lacking at both the shortest and longest periods, and northwestern Greenland has only sparse coverage at the longest periods.

3.2.1 Model resolution

We carried out a range of resolution tests to assess the reliability of the group velocity maps, using three representative periods: 25, 50 and 70 s. These three correspond to high, intermediate and low path coverage, respectively. The tests can be divided into two main types: leakage tests and synthetic tests (Fig. 5; Supporting Information Figs S2 and S3).

In the leakage tests, one component (isotropic heterogeneity, 2ψ anisotropy or 4ψ anisotropy) of the original group velocity map based on inversion of the data set is used as the starting model. A synthetic data set based on the path coverage is computed, with the

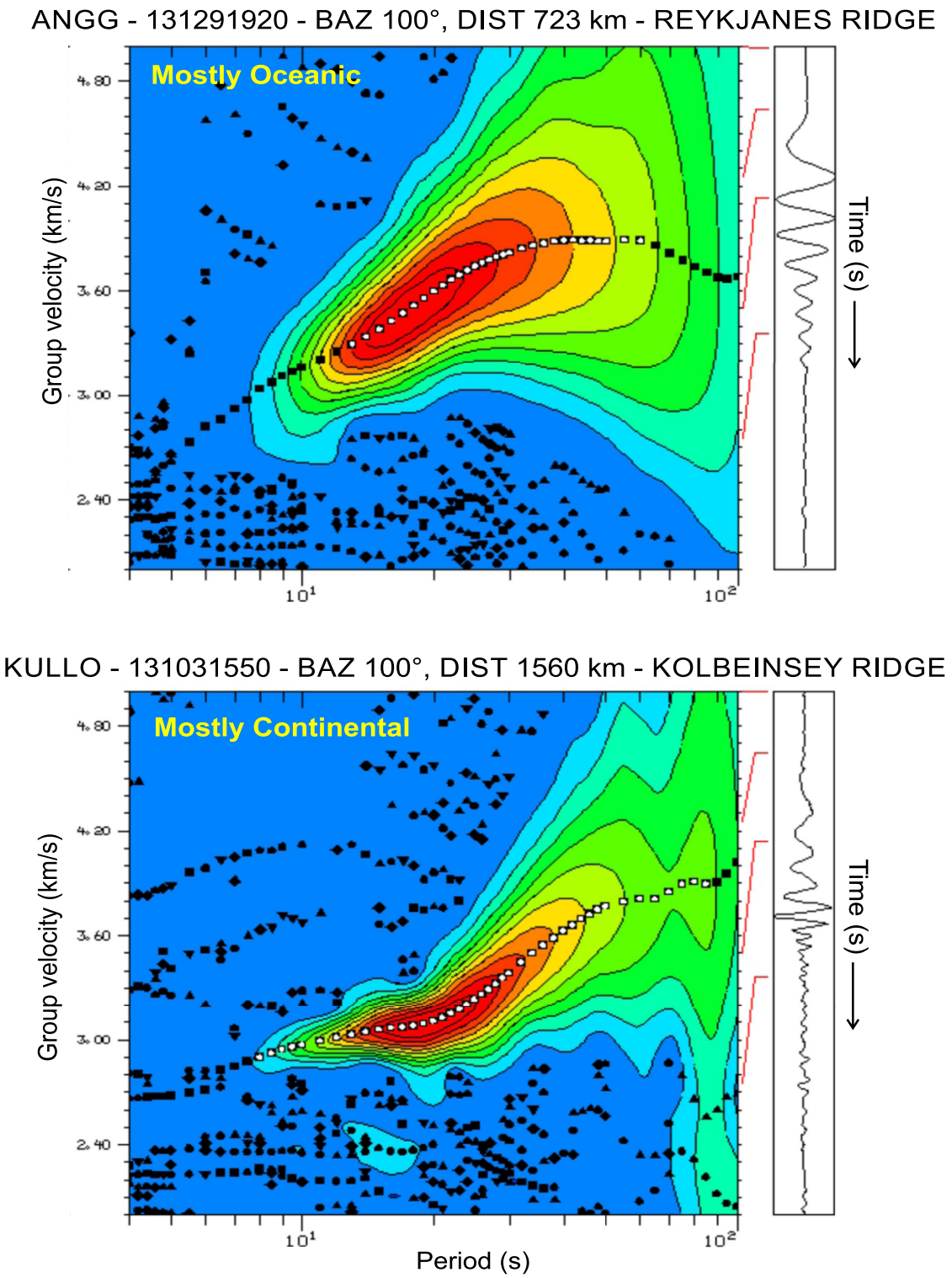

Figure 3. Examples of group velocity measurement using multiple-filter frequency–time analysis (Herrmann 2013). The coloured panel shows the energy of the surface wave envelope as a function of group velocity and period; white squares represent the maximum of the envelope picked for further analysis. The right-hand panel shows the seismogram. Two paths are plotted for comparison; the first mostly traverses oceanic lithosphere and the second mostly traverses continental lithosphere. The number after the station code is the origin time of the earthquake (*YYJJJHHMM*), BAZ, backazimuth; DIST, earthquake–station distance.

addition of a small amount of Gaussian noise, and these synthetic data are then inverted using the same regularization parameters as for the original tomography. We assessed the degree of recovery of the component tested, and the leakage into the other two components. In general we found, even for the periods with relatively sparse path coverage, that leakage was small, and mostly restricted to regions where the path coverage (density and/or azimuth) was lowest. However, at 25 s period, some leakage from isotropic

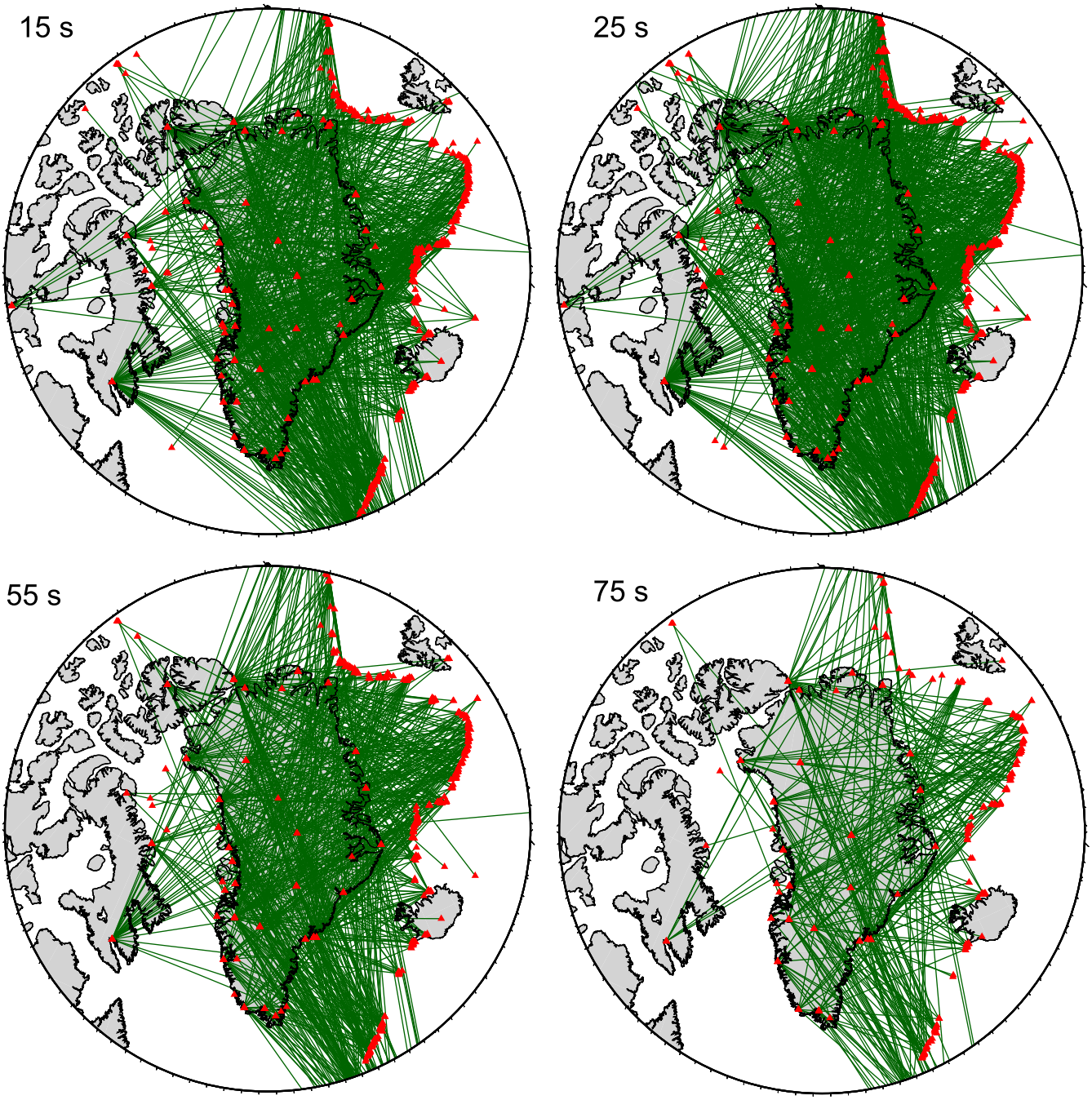

Figure 4. Path coverage of binned earthquake-station paths (green lines) at four representative periods. Stations and earthquakes are both shown as red triangles.

heterogeneity to 2ψ anisotropy was observed for the northern part of Greenland where isotropic group velocities are particularly low, and this was taken into account for the interpretation of anisotropic fabric for this region at periods corresponding to crustal depths. Negligible leakage from 2ψ anisotropy to isotropic heterogeneity was observed in this region.

Synthetic models were created by choosing sets of individual grid nodes to create low-velocity anomalies in a high-velocity background. We tested checkerboards of various sizes and distributions, sets of linear anomalies in different directions across the region, and other synthetic structures (Fig. 5). Recovery of the input anomaly shapes was generally very good wherever crossing path density was moderate to high, for all regions south of the north Greenland coast. We found that some resolution on a single-gridpoint (100 km) scale was possible in the regions of highest path coverage. Structures at a $\geq$200 km spatial scale were generally well-resolved across the region though, as is typically the case for tomographic studies with regularization, amplitude recovery was suppressed. Azimuthal anisotropy was less well-resolved, and abrupt boundaries in the checkerboard tests led to some leakage into isotropic heterogeneity. More gradual transitions, however, reduced such leakage. We estimate that changes in azimuthal anisotropy on a scale of $\sim$600 km can be well resolved.

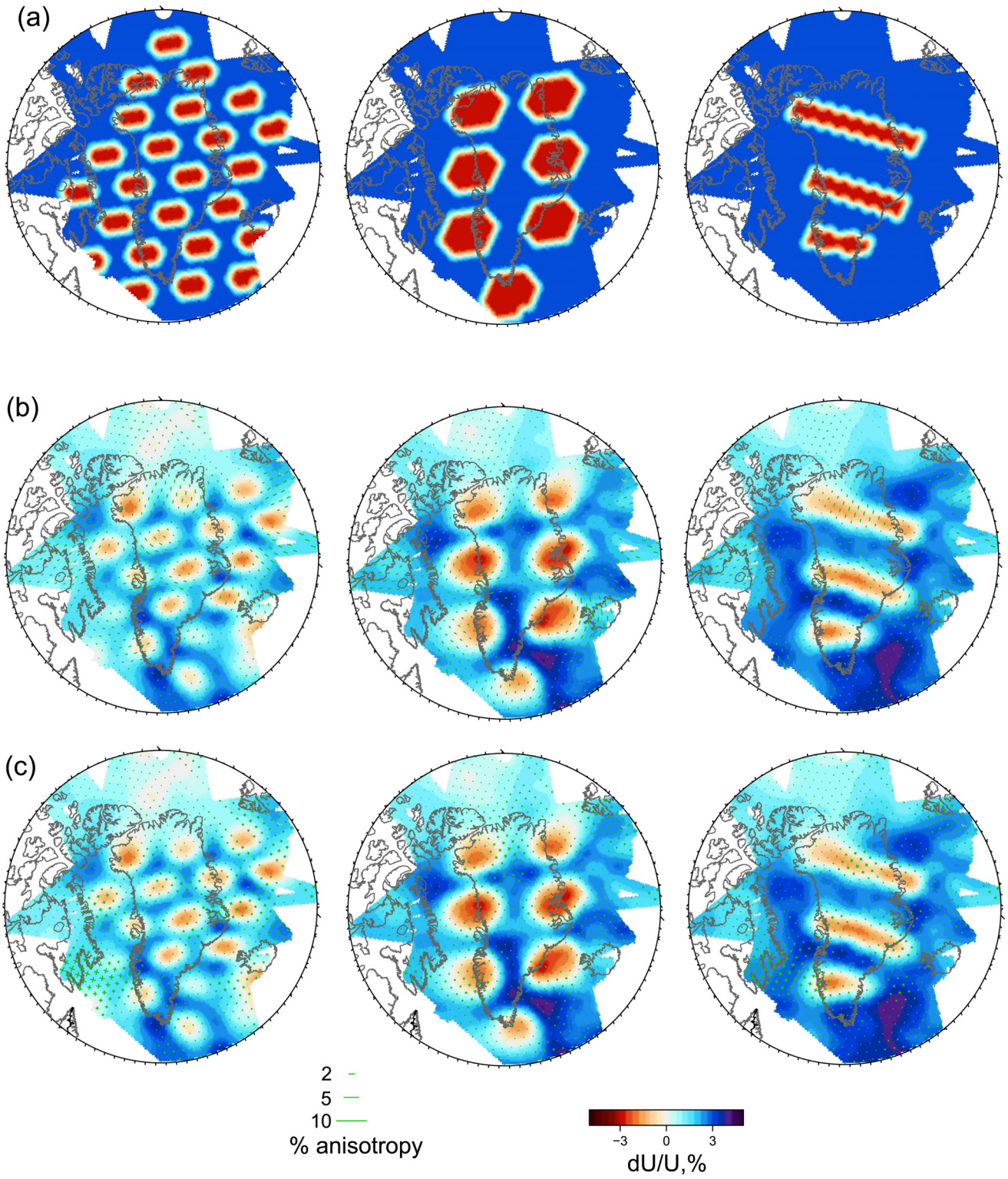

Figure 5. 'Checkerboard' and 'structural' type resolution tests for path coverage at 25 s period. (a) Input models (isotropic), (b) recovered models (isotropic plus 2ψ), (c) recovered models (isotropic plus 4ψ). Further resolution tests are shown in Supporting Information Figs S2 and S3.

3.3 Group velocity maps

Group velocities for periods between 10 and 70 s are sensitive to structure throughout the crust and into the upper mantle to ∼100 km depth (Fig. 6). It is important, however, to note that not all anomalies in the group velocity maps (Fig. 7) are controlled by crust/upper-mantle structure. The Greenland ice sheet is over 3 km thick in the central part of the continent (Amante & Eakins 2009), and water depth in the neighbouring ocean basins reaches similar values. Fig. 8 shows that a 3-km thick ice layer has a significant effect on group velocities for all periods considered in this study, lowering group velocities by as much as 0.25 km s^{-1} at 20 s period. The

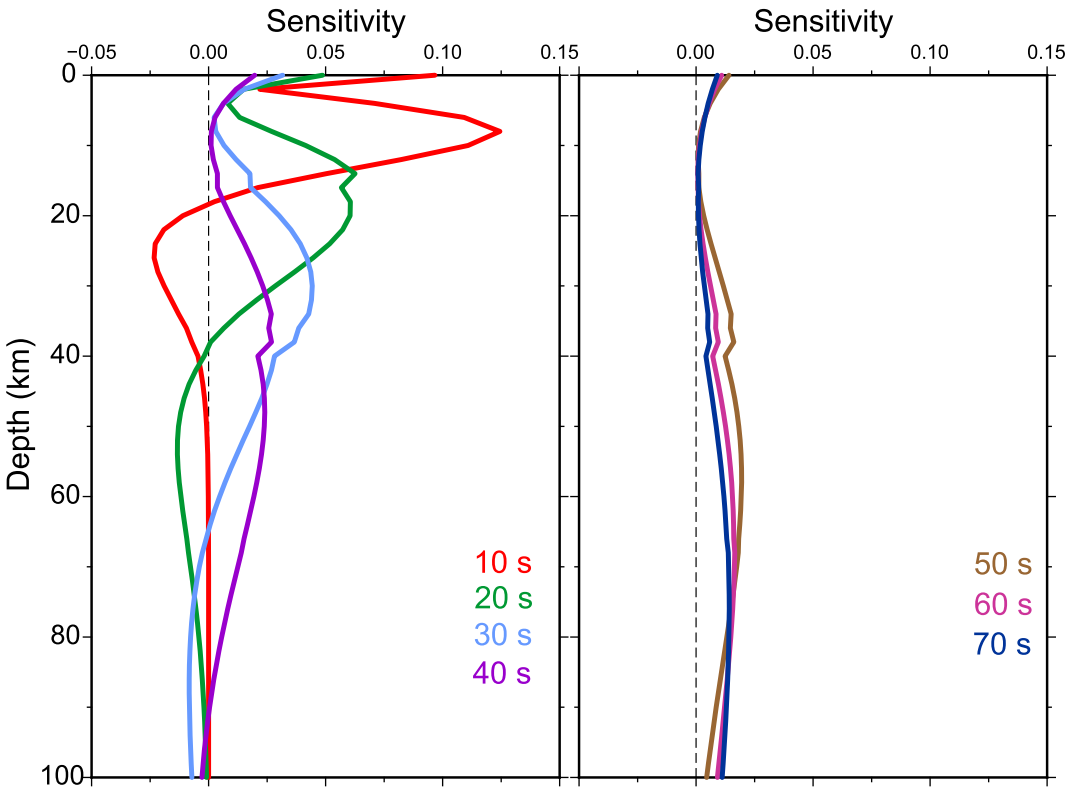

Figure 6. Rayleigh wave group velocity sensitivity kernels for periods between 10 and 70 s, calculated for a simple model with 40 km thick crust and upper-mantle velocities as for AK135.

effect is stronger, but more restricted in period range, for a water layer. Our group velocity measurements average the effects of structure along the source-station path. Earthquakes in Greenland and Arctic Canada sample continental structure that may include a variable-thickness ice layer along part of the path. Paths from mid-Atlantic earthquakes may include both a variable water depth and a variable ice thickness depending on the station location. Although tomographic inversion aims to localize velocity anomalies, the averaging inherent in the source-station dispersion curves may result in a reduction of the strength of the low-velocity anomalies in parts of inland Greenland where the ice is thickest, and this is taken into account when interpreting the shorter-period group velocity maps in particular. We include the ice or water layers explicitly in our later modelling for shear wave velocity structure.

3.3.1 Isotropic variation

At the shortest periods, 10 and 15 s, isotropic anomaly patterns change significantly (Fig. 7). While some of this apparent change may be related to the significant improvement in path coverage between the two periods, it is likely that the large-scale features are robust across Greenland. Some of the difference may arise from the changes of sensitivity to shallow structure (e.g. the inland ice) between the two periods. An E–W divide is observed at 10 s, in contrast to a more patchy N–S pattern at 15 s. The most prominent slow anomaly is a feature just off the NE Greenland coast; this persists to at least 40 s period and is likely correlated with the deep sedimentary basin apparent in compilations such as Laske & Masters (1997).

For periods of 20–40 s, the large-scale anomaly patterns are dominated by the divide between fast group velocities in the oceanic areas and slow group velocities beneath Greenland and northernmost Canada (Fig. 7). In this period range, the surface waves are primarily sensitive to depths corresponding to continental crust and oceanic upper mantle. At 20–30 s, a broad zone of particularly low group velocity covers northern Greenland, with narrower NE–SW-trending low velocities further south. In contrast, at 30–40 s, the slowest group velocities are much more localized, with five particularly strong anomalies apparent beneath the Greenland landmass. The fastest group velocity anomalies are found in the Atlantic region at periods of 20–30 s, correlated with the deepest ocean-basin regions.

The 45–55 s period range corresponds to depths at which the surface waves are likely sampling a combination of lowermost crust and uppermost mantle beneath Greenland; hence the clear continent-ocean divide is lost. The anomalies become more patchy in nature, with the strongest located beneath the Tertiary volcanic province in E Greenland, NW of Iceland (Fig. 7).

At periods of ≥60 s, path coverage becomes more sparse, therefore only the larger-scale anomalies should be treated as robust. At a broad scale, the group velocity maps again show a clear divide between continent and ocean. However the pattern is reversed from that of the intermediate periods; the Greenland subcontinental lithospheric mantle shows as a seismically fast structure, whereas the Atlantic Ocean is largely slow, particularly in the region between Iceland and Greenland. Two regions of particularly fast group velocity are observed: one covering much of northern Greenland and the other confined to the southwest (Fig. 7). Both are also visible in high-resolution global tomographic models (e.g. Schaeffer & Lebedev 2013, 2014), and the southwestern anomaly was imaged by Darbyshire *et al.* (2004) at periods of 50–80 s in their regional phase velocity study.

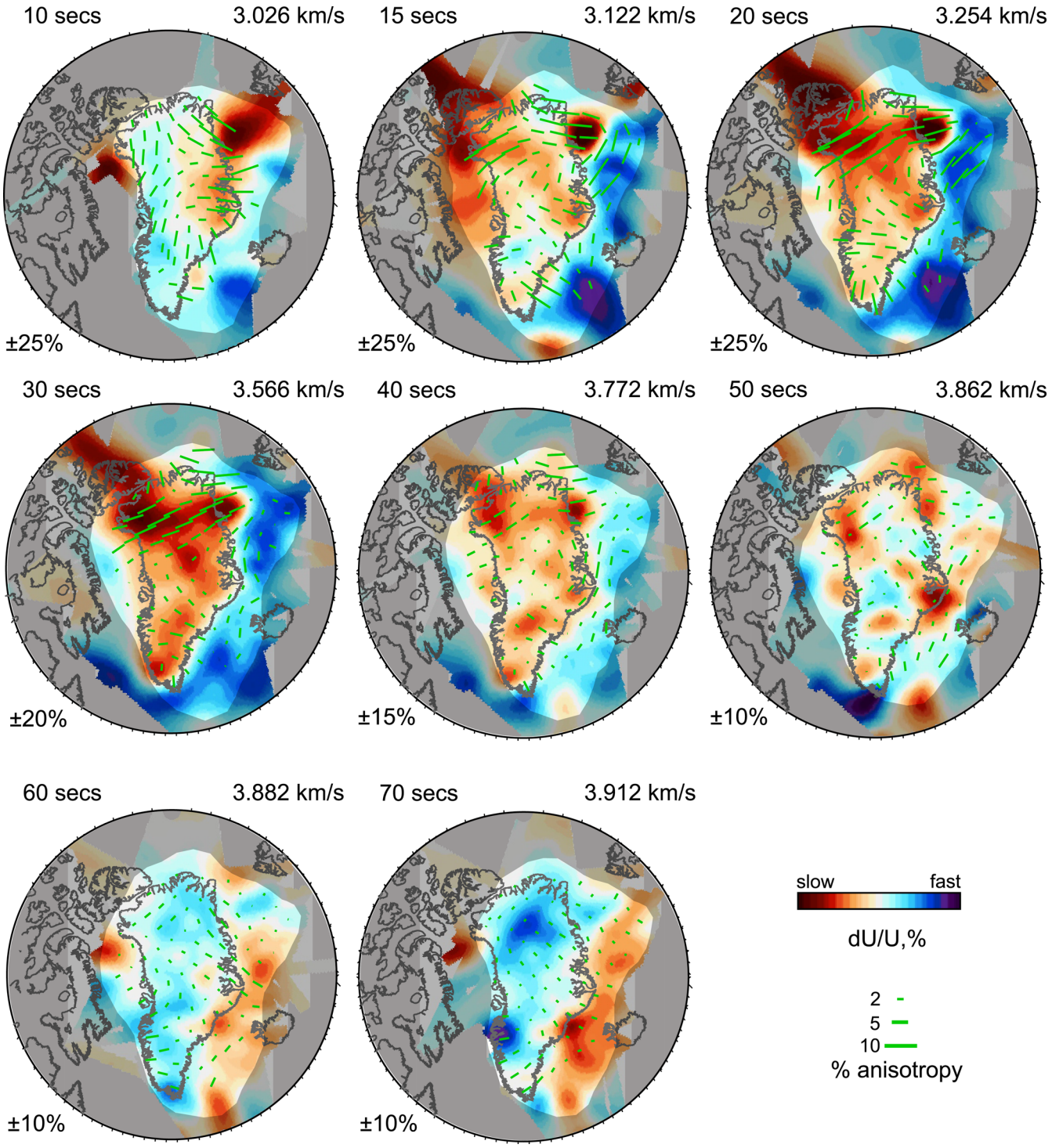

Figure 7. Group velocity maps for a subset of periods. The colour scale represents isotropic group velocity heterogeneity with respect to the regional average for the given period and the green bars show 2ψ azimuthal anisotropy. Anisotropy bars are removed in areas of the model where azimuthal coverage of paths is insufficient for a robust estimation, and a semi-transparent mask indicates areas where overall path coverage is poor or absent (*cf.* Fig. 4). Labels as follows for each map—top left: period; top right: average group velocity; bottom left: range of group velocity perturbation in per cent with respect to the mean. Further group velocity maps are shown in Supporting Information Fig. S5.

In their Arctic group velocity study, Levshin *et al.* (2001) show maps at 20 and 40 s period. Within the differences related to scale, resolution and path coverage, the two 40 s maps are mostly consistent, highlighting the continent-ocean contrast and the slow velocities beneath the northern Greenland sedimentary basins. In contrast, the 20 s map of Levshin *et al.* (2001) shows high velocities throughout western Greenland, similar to the velocities of the surrounding oceanic regions, whereas this study exhibits the lower velocities characteristic of continental crust.

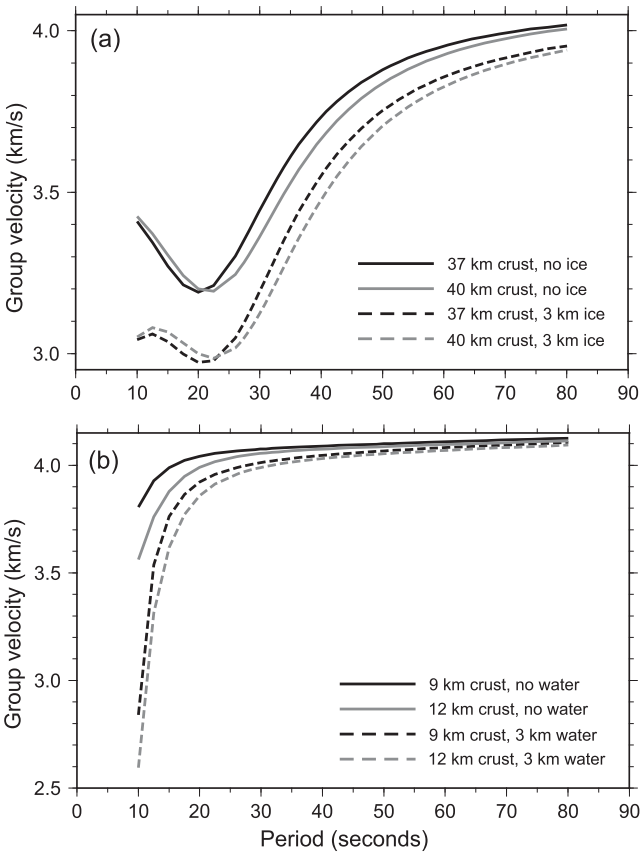

Figure 8. Effect of water/ice layers on group-velocity dispersion curves. In each case, the crust is modelled as a single layer over a half-space and a synthetic dispersion curve is calculated. Note that the effect of a 3 km water/ice layer is significantly greater than the effect of changing crustal thickness by 3 km.

3.3.2 Azimuthal anisotropy

2ψ and 4ψ anisotropy have comparable maximum amplitudes across the model (Supporting Information Fig. S4), with 2ψ anisotropy generally slightly stronger than that of 4ψ overall. In the upper mantle, it is generally considered that Rayleigh waves have low sensitivity to 4ψ anisotropy, and that high amplitudes in tomographic models indicate regions where poorer azimuthal coverage reduces model resolution (e.g. Darbyshire & Lebedev 2009). However, this is not necessarily the case in the crust, where more complex, interacting fabrics can produce both 2ψ and 4ψ symmetry observable in Rayleigh wave anisotropy.

Resolution tests (Supporting Information Figs S2 and S3) suggest that, for most of the study region, only a small amount of the observed anisotropy can be attributed to leakage between inversion parameters; the majority of the signal is therefore considered to have a structural origin. A likely exception is that of central-northern Greenland at periods 20–35 s, where leakage from an isotropic to a 2ψ signal is more significant, suggesting that the anisotropy amplitudes estimated in this region are higher than the true crustal anisotropy.

Patterns of azimuthal anisotropy variation are similar in spatial extent between the 2ψ and 4ψ components, particularly for wave periods that primarily sample depths associated with the continental crust. We therefore restrict our descriptions and interpretations to the 2ψ component.

At the shortest periods (10–15 s) azimuthal anisotropy varies significantly in both amplitude and orientation across the study region, at spatial scales of ∼500 km. Fast orientations range from NW–SE in southern Greenland and the adjoining oceanic region to E–W in central-northern Greenland and the NE offshore sedimentary basin area, to NE-SW in the northern North Atlantic. At 20–35 s, where the Rayleigh waves sample crustal material beneath Greenland and mantle material beneath the surrounding oceans, the dominant fast-orientation across the region is broadly E–W, with the exception of a more N–S fabric in northernmost Greenland. The amplitude of the anisotropy generally decreases with increasing period (Supporting Information Fig. S4). Patterns of anisotropy remain variable at longer periods (≥45 s); fast orientations appear to smooth out at periods >60 s, though this could be partially attributed to the decrease in path coverage at the longest periods (Figs 4 and 7).

4 ISOTROPIC SHEAR WAVE VELOCITY STRUCTURE

4.1 1-D modelling

At each model grid knot a group velocity dispersion curve, representing the 1-D structure beneath the knot, was extracted from the isotropic component of the group velocity maps. This dispersion curve was then inverted for 1-D shear wave velocity (V_{SV}) as a function of depth, using the method of Guo *et al.* (2016). Since the least-squares tomographic inversion (Section 3.2) does not allow the estimation of uncertainties for the group velocities, we assigned uncertainties scaled with period, in the same fashion as that used for the source-station curves input to the tomographic inversion. For the V_{SV}–depth models, we used a statistical method which expresses shear wave velocity structure and Moho depth in probabilistic terms. The model parameters and observable data are represented by a 'posterior probability density function (PDF)' (e.g. Tarantola 2005) from which information on the best-fitting models and their uncertainties can be derived. The posterior PDFs for the models are estimated using Monte Carlo sampling (e.g. Mosegaard & Tarantola 1995), implemented through the Delayed Rejection and Adaptive Metropolis algorithm of Haario *et al.* (2006). This implementation tunes the sampling of the parameter space using information from past samples of the Monte Carlo chain. After an initial stage in which a wide parameter space is sampled almost uniformly, subsequent adaptations update the distribution to narrow down the parameter space searched, and thus concentrate sampling around the regions in which the model provides a good fit (i.e. within data errors) to the dispersion data. In our study, we found that a simulation run of 40 000 samples, with an initial non-adaptive run of 20 000 samples and 5 subsequent adaptation stages, was sufficient to provide good convergence and a meaningful posterior PDF for velocity structure. Two forward-modelling methods were used to generate synthetic dispersion curves for the sampled models: the Computer Programs in Seismology package of Herrmann (2013) for grid knots on land and the MINEOS package of Masters *et al.* (2007), which handles water layers better but is more computationally expensive, for grid knots in the ocean.

In this study region, it was important to include ice or water layers explicitly in the models, as both have a significant effect on surface wave dispersion (illustrated by synthetic tests; Fig. 8). At each grid knot, we extracted the ice thickness/water depth from the NOAA ETOPO1 database (Amante & Eakins 2009) to use as a fixed top

Table 2. Previous crustal structure studies in the region, used to estimate starting model Moho depths in the current study; see Supporting Information Fig. S1. CS: continental shelf; COT: continent-ocean transition. Moho depths are in km.

Region	Experiment	References	Moho depths
SW Greenland CS		Chian & Louden (1992) Gohl & Smithson (1993) Dahl-Jensen *et al.* (1998)	30–42
SW Greenland COT		Chian & Louden (1994)	12–32
Greenland/Canada mainland	GLATIS, GLISN, NEAT, + others	Gregersen (1970) Dahl-Jensen *et al.* (2003) Darbyshire (2003) Kumar *et al.* (2007) Schiffer *et al.* (2014)	23–49
Svalbard COT		Jackson *et al.* (1984) Ritzmann & Jokat (2003) Ritzmann *et al.* (2004) Hermann & Jokat (2013)	5–32
Ocean basins		Kodaira *et al.* (1997) Døssing *et al.* (2008)	8–13
E Greenland Caledonides		Fechner & Jokat (1996) Schlindwein & Jokat (1999) Schmidt-Aursch & Jokat (2005)	21–48
E Greenland COT		Weigel *et al.* (1995) Voss & Jokat (2007) Voss *et al.* (2009)	11–32
SE Greenland COT	SIGMA	Korenaga *et al.* (2000) Holbrook *et al.* (2001) Hopper *et al.* (2003)	12–40
N Greenland CS	LORITA	Jackson & Dahl-Jensen (2010)	18–28
Nares Strait		Reid & Jackson (1997) Funck *et al.* (2006)	16–36
Baffin Bay		Jackson & Reid (1994) Reid & Jackson (1997) Funck *et al.* (2012) Suckro *et al.* (2012)	12–37
Davis Strait	NUGGET + others	Funck *et al.* (2007) Gerlings *et al.* (2009) Suckro *et al.* (2013)	17–24

layer in the starting models. Synthetic tests showed that the group velocity curves are insensitive to ice/water layers of 100 m or less, so the starting models were assigned ice/water layers of either zero thickness or increments of 100 m thickness from 0.1 to 3.7 km. The water layer was assigned a *Vp* of 1.5 km s^{-1}, *Vs* of 0.0 km s^{-1} and density of 1.0 g cm^{-3}. Following Dahl-Jensen *et al.* (2003) and references therein, the ice layer was assigned seismic velocities of 3.81 and 1.92 km s^{-1} (*Vp*, *Vs* respectively) and a density of 0.91 g cm^{-3}. Seismic *Q*-factors for the ice layer were estimated from an average of values for Greenland and Antarctica compiled by Peters *et al.* (2012).

Each starting model was parametrized as follows: the ice/water layer (if applicable), 2–4 cubic B-splines for V_{SV} in the crust and 5 cubic B-splines for V_{SV} in the mantle, to a maximum depth of 250 km. To provide initial *a priori* constraints on Moho depths, we used published values from previous seismological studies (see Table 2 and Supporting Information Fig. S1 for details) and interpolated between them, also using bathymetry as a guide. A range of Moho depths of ±15–20 km around the initial estimates was used to constrain each model. Seismic *Q*-factors in the crust and upper mantle were taken from PREM (Dziewonski & Anderson 1981), with an added zero-*Q* layer for the oceanic grid points. Changes in crustal or upper-mantle *Q* in the starting parameters made negligible difference to the output models, with differences in velocity-depth profiles and Moho depths within the standard deviations of the model sets. *Vs* was constrained to increase with depth at the base of the ice/water layer and at the Moho. We allowed low-velocity zones in the continental crust, but not in the oceanic crust. For each grid knot, we obtained a posterior PDF for velocity–depth structure and a probabilistic estimate of Moho depth (Fig. 9).

Following 1-D inversion at each grid point, the mean V_{SV} model was corrected for elevation where applicable, to standardize all models to be at sea level at zero depth. Standard gridding algorithms (Wessel & Smith 1998) were then applied to construct a pseudo-3-D model from the 1-D results.

4.2 Results: 3-D crust and uppermost-mantle structure

The pseudo-3-D models show, on the broadest scale, the expected division of crustal structure between oceanic and continental regions. This is particularly apparent at the 25–35 km depth ranges, where shear wave velocities are <4.2 km s^{-1} across almost all of the continent, with only isolated parts of the oceanic regions exhibiting similarly low values. By ∼45 km depth, almost all of the continental region exhibits shear wave velocities typically associated with the mantle, reflecting the observed range of crustal thicknesses (∼25–55 km) across most of Greenland (Figs 10 and 11).

In the mid-crust, the strongest features are a set of low-velocity anomalies across the northern half of Greenland. These are particularly strong just offshore NE Greenland, where an extensive sedimentary basin is situated, but also across the NW

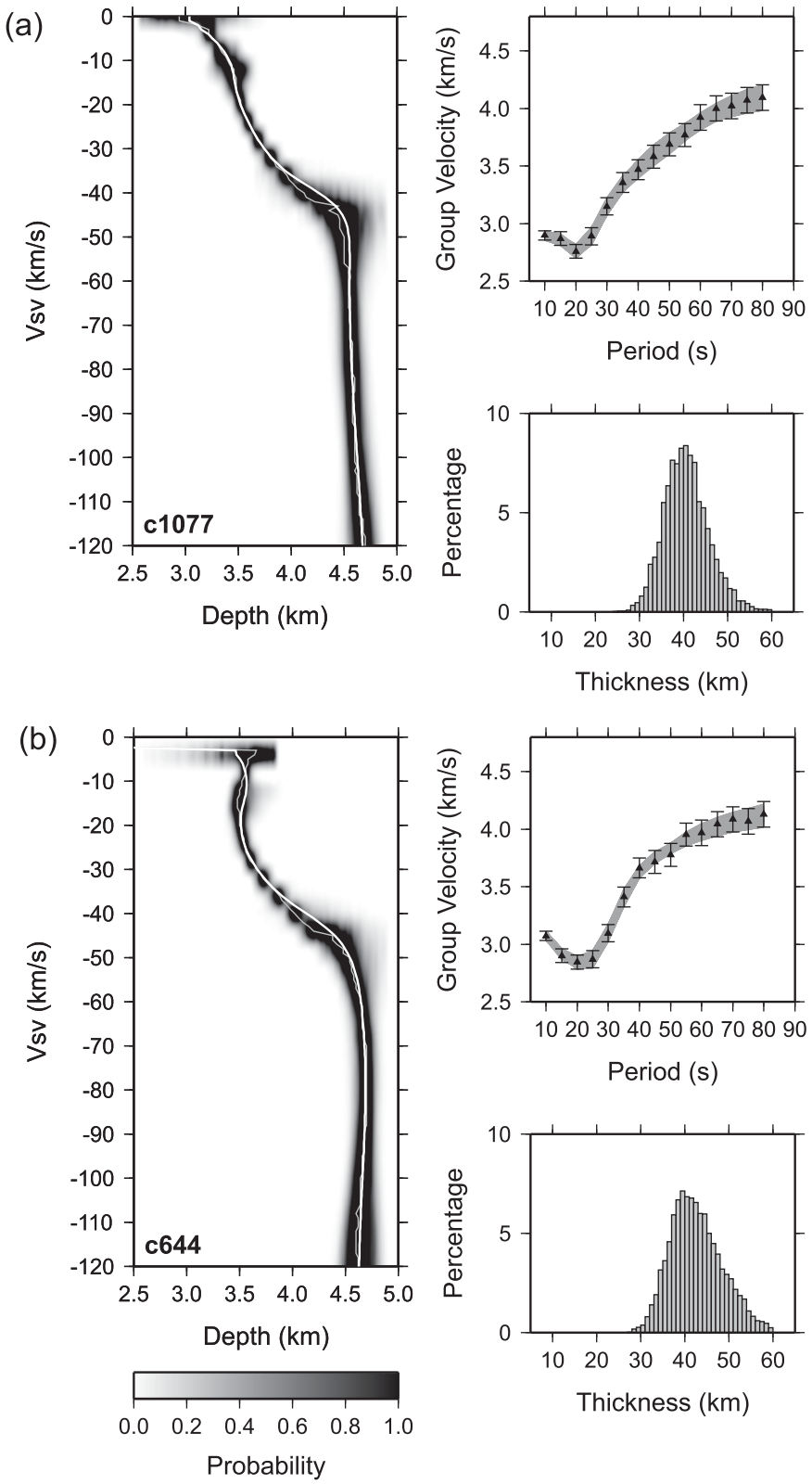

Figure 9. Examples of 1-D inversions for (a) a site on rock, (b) a site with a 2.5 km ice layer. Left: velocity-depth model, shown with respect to the probability of fitting the group velocity data. The thin light grey line is the best-fitting individual model and the thick white line is the mean velocity-depth profile. Top right: dispersion data (triangles with error bars) and the ensemble of synthetics (grey lines) from accepted models. Bottom right: probability-density function (PDF) for crustal thickness. In the PDF, the 'Moho' is defined as the depth in the model where a positive velocity jump is most likely, also marking the transition in the model from the 'crustal' to the 'mantle' splines.

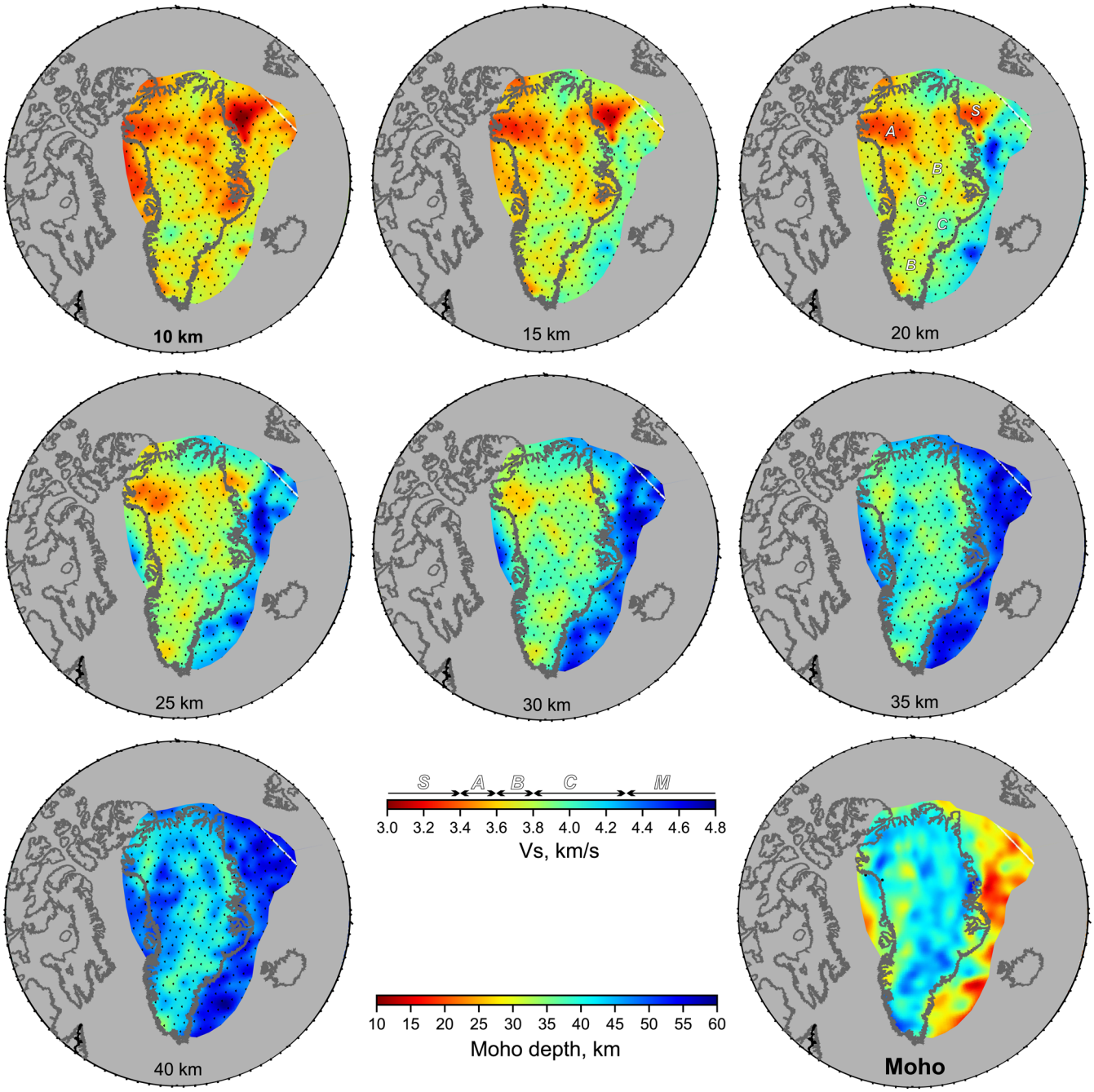

Figure 10. Depth slices through the model from 10 to 40 km depth. The colour scale is chosen to highlight lateral variations within the crust, with typical mantle velocities ($\geq$4.3 km s^{-1}) shown in blue. Velocities corresponding to sedimentary structures ('S'), crustal layers A–C and mantle ('M') are indicated on the 20 km depth slice and the velocity scale bar. Bottom right: Moho depth map for the region.

part of the continental landmass. More isolated, weaker anomalies are observed in central-eastern regions, particularly beneath the east coast around the Scoresbysund region (surrounding station SCO; Figs 1 and 10). The northern anomalies persist well into the lower crust (~30 km), whereas velocities are fast with respect to the Greenland average at depths of >30 km beneath Scoresbysund.

The uppermost mantle beneath most of Greenland (depths of 55 km and greater) is characterized by shear velocities significantly higher than the global average of 4.48–4.50 km s^{-1} (e.g. AK135; Kennett *et al.* 1995), consistent with the presence of a cold, depleted lithospheric keel. This high-velocity zone extends well beyond the coast in the NE, showing a lobe of high-velocity material to at least 100 km depth (the base of resolution of the model). In contrast, most of the rest of the oceanic region shows velocities significantly lower than the global average, both close to the mid-ocean ridge system and extending slightly inland of the SE Greenland coast (Fig. 11). The highest velocities are observed in central-eastern and southernmost Greenland, separated by a band of slightly lowered velocities in the south.

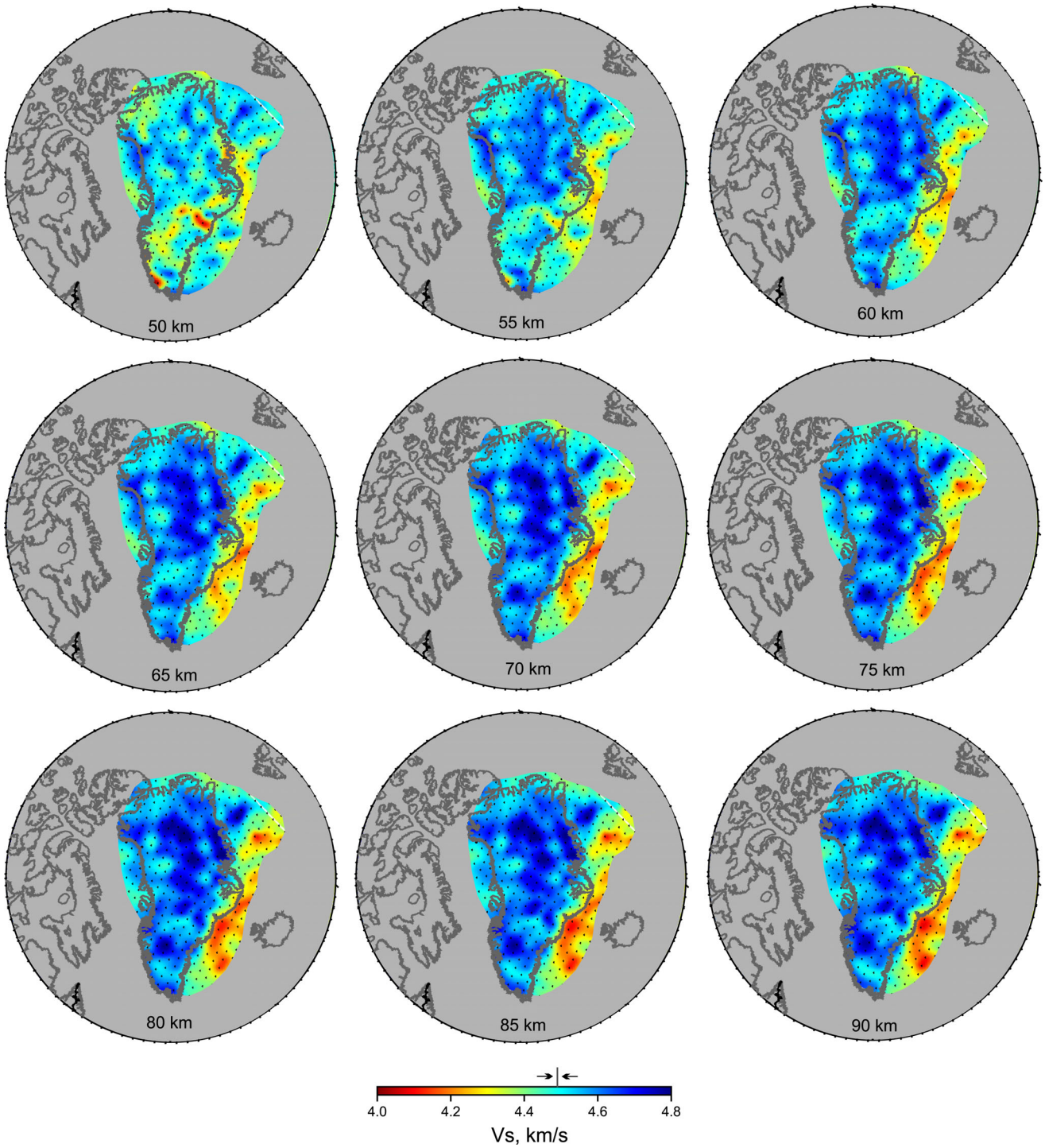

Figure 11. Depth slices through the model from 50 to 90 km depth. The colour scale is chosen to highlight lateral variations within the mantle, with velocities of $\leq$4.2 km s^{-1} shown in red. The dark grey bar and double arrow above the colour scale indicate the range of velocities from the AK135 global reference model for these depths.

5 DISCUSSION

5.1 Crustal thickness

Beneath the Greenland landmass and much of the continental shelf region, the surface wave model is broadly consistent with previous seismological studies, with crustal thicknesses in the ∼25–50 km depth range, with a mean Moho depth of 40 ± 6 km.

Crustal compilations, such as the EUNAseis model of Artemieva & Thybo (2013) and CRUST1.0 (Laske *et al.* 2013) show similar ranges, as do crustal thicknesses inferred from global gravity models (e.g. Gaina *et al.* 2014) and point-estimates from receiver function analysis (Dahl-Jensen *et al.* 2003; Kumar *et al.* 2007).

Gravity-based models of Greenland crustal thickness (e.g. Braun *et al.* 2007; Gaina *et al.* 2014; Petrov *et al.* 2016; Steffen *et al.* 2017) suggest crustal thinning beneath much of northern Greenland. At

a regional scale, details vary between models, notably for the southern part of the Archean block and for the Ketilidian crust in the far south of Greenland. Our surface wave model does not show the region-wide crustal thinning across northern Greenland. Other patterns of Moho depth variation across the rest of Greenland do not correlate well with the model of Braun *et al.* (2007), but are in better agreement with the Steffen *et al.* (2017) model; notably the deep Moho on parts of eastern and southern Greenland. We note that Braun *et al.* (2007) reconcile a discrepancy between gravity and receiver function based Moho depths in SW Greenland via a local change in lower-crustal density, and therefore speculate that much of the difference between the surface wave and gravity based crustal thicknesses can be attributed to the significant heterogeneity we find within the crust (Section 5.2). In particular, a density-thickness trade-off in northern Greenland may explain the discrepancies between the seismic and gravity models.

Across the Greenland continental margins and regions of oceanic crust, the consistency between the surface wave model and results from refraction profiles is less clear. There is relatively good agreement in patterns of crustal thickness variation offshore central-east Greenland, the thick crust of the Greenland-Iceland Ridge, the central SE margin and the parts of the Baffin Bay margin that are resolved by our study. Results are, however, inconsistent for the SE Greenland margin (SIGMA3 profile; Holbrook *et al.* 2001) and for the oceanic crust in the central North Atlantic. In the former case, the transition from crust to mantle may be complicated by the presence of extensive mafic intrusions in the lower crust of the volcanic rifted margin. Our surface wave study infers a Moho depth from a gradual transition from 'typical' crustal to mantle velocities, whereas refraction studies rely mainly on wide-angle reflections from a sharp Moho. In a heavily intruded region, shear wave velocities intermediate between those of the continental crust and the upper mantle are common, and the Moho may vary in character, leading to Moho depth discrepancies even though both the refraction and surface wave studies have good resolution. In the central Greenland Sea, the thinnest crust ($\leq$5–10 km) is likely below the resolution limit of the periods used in this study, resulting in a greater apparent crustal thickness in the current model.

5.2 Crustal heterogeneity

There is little prior information on seismic velocity variations within the Greenland crust, aside from a few seismic refraction profiles that penetrated inland eastern Greenland (e.g. Schmidt-Aursch & Jokat 2005). However, *Vp*/*Vs* ratios from receiver functions suggest a largely felsic bulk crustal composition for most parts of Greenland (Dahl-Jensen *et al.* 2003; Kumar *et al.* 2007). The absolute shear wave velocities inferred from the surface wave modelling in this study are also consistent with a broadly felsic crystalline crust across much of the landmass.

The crustal depth slices (Fig. 10) show a considerable amount of heterogeneity in crustal velocities across Greenland and its surroundings. In order to characterize these results, we reviewed the velocity models for coastal Greenland from refraction profiles (Table 2) and used a simple Poisson solid assumption to estimate equivalent shear wave velocities. Based on this compilation, we divide the model as follows: (i) *Vs* $<$3.4 km s^{-1}: sedimentary structures, (ii) *Vs* 3.4–3.6 km s^{-1}: upper crystalline crust—Layer A, (iii) *Vs* 3.6–3.8 km s^{-1}: middle crust—Layer B, (iv) *Vs* $>$3.8 km s^{-1}: lower crust and transition towards mantle velocities—Layer C.

The lowest seismic velocities, most likely associated with sedimentary structures, are found offshore NE Greenland (notably the deep Danmarkshavn-Thetis basin Henriksen *et al.* 2009), beneath parts of the eastern coastal areas such as the Jameson Land Basin region and in the offshore region between east Greenland and NW Iceland. These offshore basins are prominent features in global models such as CRUST1.0 (Laske *et al.* 2013), and a recent compilation of Arctic-region data (Petrov *et al.* 2016), in which sediment thicknesses offshore NE Greenland reach $\sim$15–18 km.

Layer A, with velocities associated with the upper or upper-mid crystalline crust in seismic refraction profiles, is extremely variable in its occurrence and its thickness across Greenland (Figs 10, 12 and 13). In some regions of SW Greenland this layer is too thin to be resolved by the tomographic model, whereas it extends to $\sim$20–25 km depth across much of northern and central-eastern Greenland. Across the southern half of Greenland, Layer A velocities are largely absent below $\sim$10–15 km, with the exception of the SW tip of the landmass, where Layer A extends to $\sim$22 km depth. By $\sim$30 km depth, the low velocities are present only beneath NW Greenland. At 10–15 km depth, Layer A appears to terminate fairly sharply between northern and central/southern Greenland along a broadly NW-SE trending boundary, though the geographic distribution of velocities becomes much less linear and more patchy below $\sim$15 km depth. Intriguingly, this NW–SE trend of reduced velocities in the upper 10–15 km correlates spatially with a region of anomalously high heat flux at the rock surface, as reported by Rogozhina *et al.* (2016). They attribute the thermal anomaly to contributions from the Iceland plume, citing apparent lithospheric erosion in the same region, deduced from seismic body wave tomographic images at $\geq$100 km depth (e.g. Jakovlev *et al.* 2012; Rickers *et al.* 2013).

The thicknesses of crustal layers B and C are likewise highly variable. In southern Greenland, cross-sections (Figs 12 and 13) show relatively simple structures, with the A–B–C boundaries largely subparallel, and dominated by the transitions from continental to oceanic crust. In contrast, in central Greenland the boundaries change significantly in depth across both the E–W and N–S cross-sections (Figs 12 and 13), with the thickest Layer B almost 20 km thick beneath parts of central-NW Greenland (cross-section B–B′; Figs 12 and 13) and the thickest Layer C of 20–25 km thickness beneath central Greenland (cross-sections C–C′ and S–N; Figs 12 and 13). The prevalence of high crustal shear wave velocities along cross-section C–C′ occurs in a region between the two significant outcroppings of Palaeogene plateau basalts associated with the breakup of the North Atlantic (e.g. Henriksen *et al.* 2009). Some continuity of this volcanic province across mainland Greenland has been proposed (e.g. Dawes 2009), and the presence of mafic intrusives in the crust might explain the higher-than-average velocities across central Greenland.

For velocities associated with the crystalline crust, we do not generally observe a significant spatial correlation between the patterns of lateral velocity variation and the primary (Precambrian and Palaeozoic) tectonic structure of mainland Greenland as inferred from its coastal geology (Henriksen *et al.* 2009), potential-field data (e.g. Verhoef *et al.* 1996; Dahl-Jensen *et al.* 2003) or inferences of tectonic subdivisions beneath the icecap (Dawes 2009). Instead, there seems to be as much crustal heterogeneity within known tectonic domains as there is between them. One possible exception is the updoming of Layer B at $\sim$600–800 km distance along profile A–A′ (Figs 12 and 13) which is spatially coincident with the $\sim$3.4 Ga Archean Victoria domain inferred by Dawes (2009) from

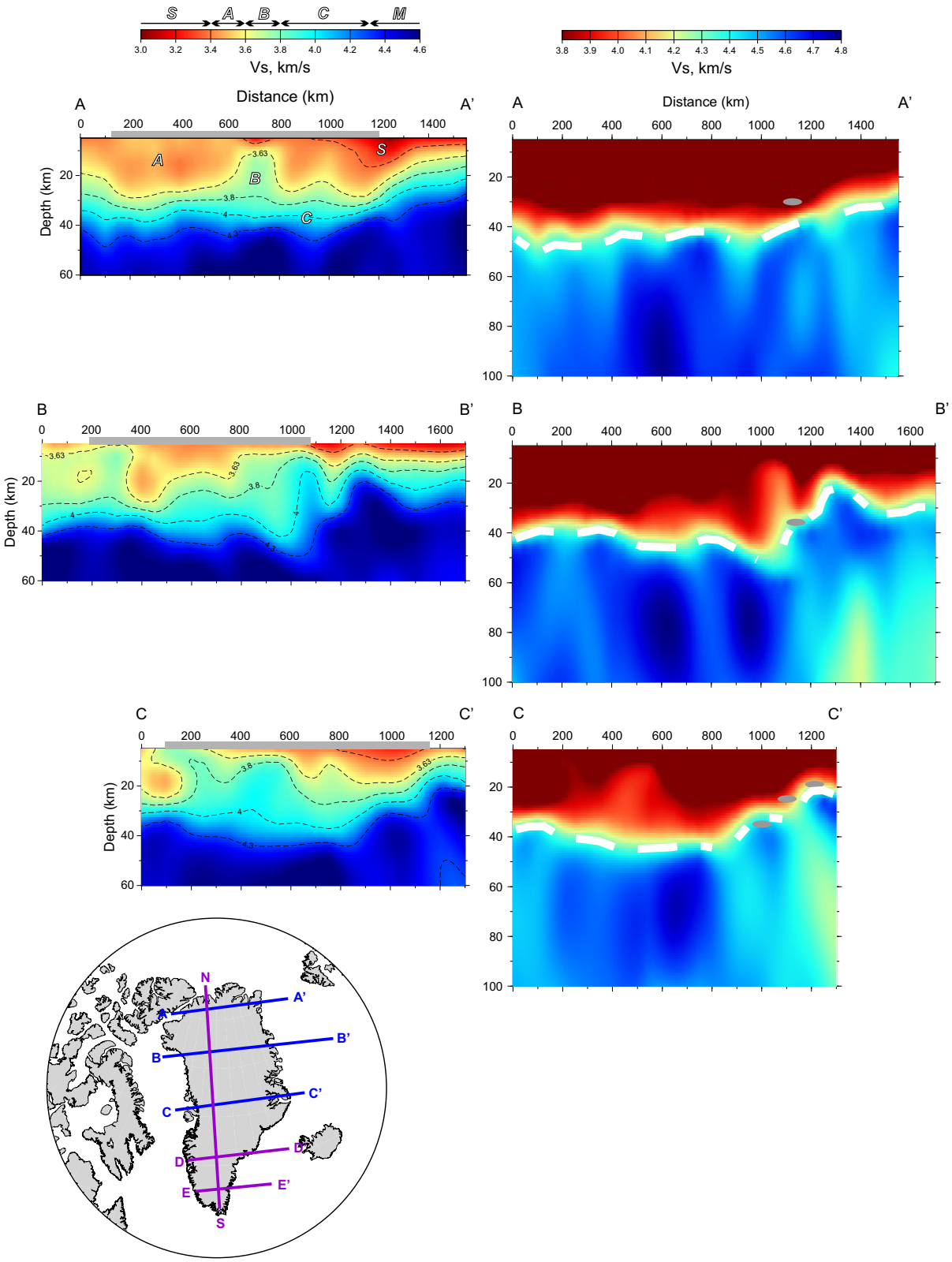

Figure 12. Cross-sections through the model for 3 E–W profiles. The transects are shown with two different colour scales and two different depth scales to emphasize crust and mantle heterogeneities separately. The contour of $Vs = 4.3\,\mathrm{km\,s^{-1}}$ is shown on the right-hand sections as a proxy for crustal thickness, and internal crustal wave-speed boundaries are marked on the left-hand sections. The thin grey bar at the top of each crustal section shows the position of the Greenland landmass. Moho depth values from previous receiver function and seismic-refraction studies (Table 2 and Supporting Information Fig. S1) are shown as grey ellipses on the right-hand sections. A, B, C: crustal layers as described in Section 5.2; S: sedimentary basins; M: mantle-type velocities. Blue lines on the map indicate cross sections shown in the figure.

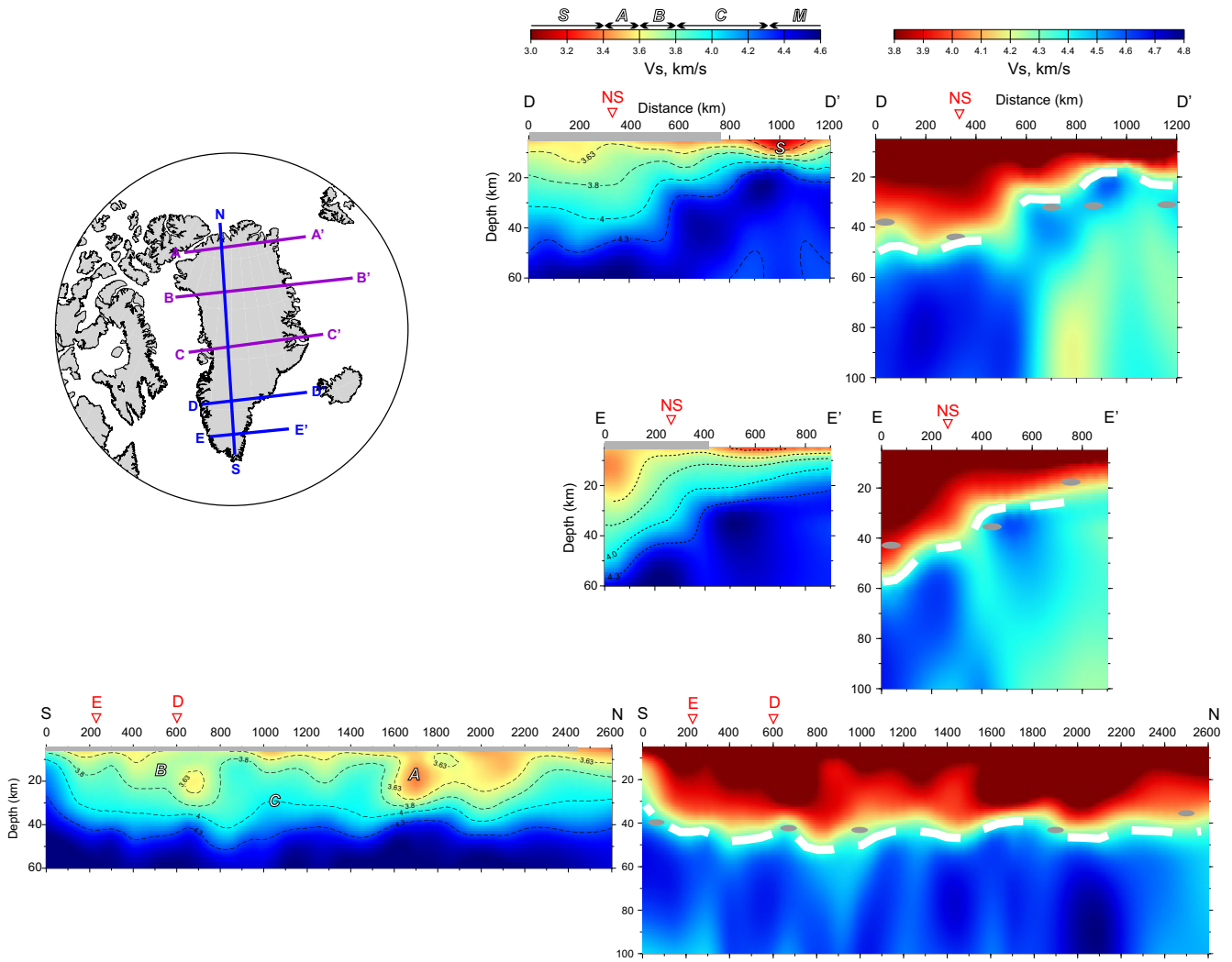

Figure 13. Cross-sections through the model for one N–S profile and 2 E–W profiles. Plotting conventions as for Fig. 12. Inverted triangles with red outline mark the intersections between the north–south and east–west profiles. Blue lines on the map indicate cross sections shown in the figure.

zircon data reported for Victoria Fjord by Nutman *et al.* (2008). The lack of direct constraint on crustal geology across the majority of the continent remains a significant challenge to the interpretation of geophysical data such as the crustal velocity structure. The N–S crustal cross-section (Fig. 13) nevertheless suggests a large-scale threefold division of the inland region, based on the distribution of velocities. The central third of the profile, thought to be underlain largely by Palaeoproterozoic material (Dawes 2009), exhibits consistently higher velocities than the regions to the north and south, both of which are associated with Archean blocks. In contrast, the N–S-trending Caledonian fold belt of eastern Greenland exhibits too much internal heterogeneity to be distinguished from the presumed Precambrian crust to the west.

5.2.1 Comparison with other stable continental regions

Lateral variations in crustal shear wave velocity within the stable continental crust (i.e. regions underlying Precambrian or Palaeozoic surface geology) range from as little as 5 per cent in the North American midcrust (e.g. Bensen *et al.* 2009; Shen & Ritzwoller 2016) to 20–30 per cent in the Australian crust (e.g. Salmon *et al.* 2013). 10–15 per cent lateral shear wave velocity variations throughout the crust are resolved across Greenland in this study. The continental Moho depth range (∼25–55 km) is also consistent with that of stable continental interiors worldwide, where Moho depths typically vary from ∼25 km to ∼60 km [such as North America (e.g. Bensen *et al.* 2009; Kao *et al.* 2013; Shen & Ritzwoller 2016), Australia (e.g. Salmon *et al.* 2013), China (e.g. Guo *et al.* 2015; Shen *et al.* 2016), Eastern Europe and Fennoscandia (e.g. Artemieva & Thybo 2013, and references therein), India (e.g. Singh *et al.* 2015) and east Antarctica (e.g. An *et al.* 2015)]. Some global-scale compilations (e.g. Durrheim and Mooney 1991; Abbott *et al.* 2013) suggest a direct link between surface crustal age and crustal thickness variations, but regional-scale studies suggest that a simple relationship of this type is by no means ubiquitous. In contrast, many regions exhibit as much crustal variation within a given tectonic age range (e.g. Archean, Proterozoic, Palaeozoic) as between the units of different ages, though the thickest crust is often correlated with regions of Proterozoic surface geology (e.g. Salmon *et al.* 2013; Petrescu *et al.* 2016; Darbyshire *et al.* 2017).

5.3 Upper-mantle structure

At mantle depths, there is a clear division between high shear wave velocities (≥4.6 km s^{-1}) beneath Greenland and its NE continental

margin, and low velocities ($\leq$4.3 km s^{-1}) beneath the North Atlantic and SE Greenland margin (Fig. 11). These results are consistent with findings from larger-scale body- and surface-wave tomographic studies (e.g. Jakovlev *et al.* 2012; Rickers *et al.* 2013; Schaeffer & Lebedev 2014; Lebedev *et al.* 2017). The high seismic velocities beneath Greenland suggest a well-developed depleted cratonic keel, whose vertical extent of $\geq$120 km (e.g. Darbyshire *et al.* 2004; Schaeffer & Lebedev 2014; Lebedev *et al.* 2017) is greater than the limit of depth resolution of our model.

Similar to the crustal portion of the model, the distribution of seismic velocities beneath the Greenland landmass does not appear to vary ubiquitously with surface tectonic domain. At depths of ~60 km and greater, the highest velocities appear beneath a broad region of central-eastern Greenland and a more isolated region of south Greenland (Figs 11–13). These regions are also observed as two separate high-velocity bodies in the lower-resolution studies of Schaeffer & Lebedev (2014) and Lebedev *et al.* (2017). The southern Greenland high-velocity anomaly was also reported by Darbyshire *et al.* (2004) in their regional study of upper-mantle structure. Comparison with surface tectonics suggests that the E–W band of slightly lowered velocities coincides spatially with the NMB and AMB (Fig. 1) and that the highest velocities underly the Archean NAC (Fig. 1). Such a direct correlation is more difficult to establish for the more northern high-velocity body due to a paucity of surface geological information for this region, and the highest velocities also appear to extend further east beneath the Greenland Caledonides. The correlation between Archean-Proterozoic surface tectonics and systematic velocity variations within a regional cratonic root has been observed in other shield regions worldwide (e.g. Lebedev *et al.* 2009), including northern Canada, which preserves a distinct seismic signature of the Palaeoproterozoic Trans-Hudson Orogen with respect to the adjoining Archean cratons (Darbyshire *et al.* 2013).

Upper-mantle velocities are particularly low ($<$4.3 km s^{-1}) beneath the western North Atlantic between the Iceland region and the SE Greenland coast. In this region, the oceanic crust is younger than 60 Ma, suggesting lithospheric thicknesses of $<$75 km according to standard plate-cooling models. In addition, the Iceland hot spot is thought to elevate mantle temperatures across much of the North Atlantic, acting to decrease mantle shear wave velocities further.

No clear correlation is visible between variations in seismic velocity and the proposed track of the Iceland hot spot across central Greenland. One possible explanation is that the hot spot was only able to modify the crust and upper lithospheric mantle at the edges of the continent, where the extensive plateau basalts are observed. The thick, cold, depleted lithosphere of cratons has been shown to be resistant to hot spot modification, and plume material is more likely to be deflected towards regions of locally thinner lithosphere (e.g. Sleep 1997, 2003). While thermal erosion of the Greenland lithosphere by the Iceland hot spot remains a plausible hypothesis, there is no evidence from this study of pervasive modification of the lithosphere above ~80–90 km depth. It may be that the strong cratonic lithosphere was resistant to modification above these depths, with only the lower lithosphere being affected by thermal erosion. This hypothesis would explain the lack of a distinct signature in this study while the tomographic models of Schaeffer & Lebedev (2014); Lebedev *et al.* (2017) indicate a corridor of reduced velocity across central Greenland between two regions of particularly high velocity for depths between ~80 and ~150–200 km depth.

5.4 Seismic anisotropy

Upper-crustal seismic anisotropy is generally attributed to alignment of vertical cracks (Crampin 1981, 1994) or other vertical features (such as dykes) in a plane. In the case of a cracked medium, the fast-polarization orientation of the anisotropy is parallel to the principal orientation of the cracks, also corresponding to the maximum compressive stress direction (Crampin 1994). Deeper in the crust, where cracks will have closed due to higher-pressure conditions, the dominant contribution to seismic anisotropy is thought to be the foliation/lineation of metamorphic rocks, which results in alignment of intrinsically anisotropic minerals such as micas and amphibole (e.g. Brocher & Christensen 1990; Meltzer & Christensen 2001). While a single plane of cracks or foliation will give rise to anisotropy with 2ψ symmetry, more complex structures such as perpendicular sets of cracks or superposition of mineral alignments resulting from different stages of deformation can be responsible for 4ψ symmetry in crustal anisotropy. In the lithospheric mantle, 2ψ anisotropy is thought to dominate for Rayleigh waves, resulting largely from lattice-preferred orientation of olivine crystals in response to large-scale deformation (e.g. Silver & Chan 1991).

Given Greenland's tectonic history, and the nature of the rocks exposed at the continent edges, large-scale metamorphic foliation is a strong candidate to explain the majority of the observable crustal anisotropy. In regional-scale studies of continental crustal azimuthal anisotropy [e.g. central and western US; Lin *et al.* (2011); Lin & Schmandt (2014), northern Canada; Pawlak *et al.* (2012), Tibet; Yao *et al.* (2010)], the fast-orientations are generally observed to correlate with tectonic provinces and major known structural alignments. The paucity of information on Greenland geology inland of the coastal regions makes such a comparison more difficult in this study, but some speculative correlations are possible using the group-velocity maps (Fig. 7) and their range of depth sensitivities (Fig. 6).

At periods $\leq$25 s, abrupt changes in fast orientation occur between NMB and AMB (Fig. 1) and the NAC (Fig. 1). A similar location for a significant change in crustal fabric is observed in magnetic anomaly maps (e.g. Gaina *et al.* 2014; Petrov *et al.* 2016). At lower-crustal depths, fast orientations are dominantly ENE–WSW in northern Greenland, rotating to WNW–ESE in the south, suggesting changes in fabric that could be correlated with the spatial distribution of reworked Archean versus juvenile Palaeoproterozoic crust (e.g. Henriksen *et al.* 2009). Fast orientations in eastern Greenland remain predominantly E–W, perpendicular to the strike of Caledonian structures (Fig. 7). Although at the edge of resolution of this study, there are indications of a rotation of fast orientations that correlate with the extensive fold belts in northern Greenland.

Offshore, beneath Baffin Bay and much of the North Atlantic, the Rayleigh waves are likely sampling oceanic mantle even at the shorter periods (10–15 s) of the study. Fast orientations are largely ridge-perpendicular, with the exception of a rotation in orientation coincident with the thick crust of the Greenland-Iceland Ridge (Fig. 7).

The Greenland lithospheric mantle, imaged by group velocities of periods $>$45 s, exhibits weaker azimuthal anisotropy than the crust, and fast orientations vary on a larger spatial scale, with a predominant NW–SE fast orientation across much of the continent. The anisotropy reflects 'frozen' or 'fossil' fabric, and is likely related to a number of different episodes of tectonic deformation during the assembly and evolution of the present-day continent (Fig. 7).

Previous regional or global-scale studies including azimuthal anisotropy vary significantly in their results. At 50 km depth, global

models show NW–SE or E–W fast orientations across mainland Greenland (Schaeffer *et al.* 2016, and references therein), though grid points are widely spaced. This is similar to the dominant fast orientations in southern Greenland at 40 s period in our studies, though our study shows significant smaller-scale variation. A predominance of NW–SE fast orientations continues to longer periods in this study, in contrast to the NNE–SSW orientation inferred by Pilidou *et al.* (2005) at 75 km depth (equivalent to ∼60–75 s period). The Arctic-wide group velocity study of Levshin *et al.* (2001) shows fast orientations at 50 s period with strong and moderate damping. In the former case, the entire Arctic region exhibits the same NE–SW fast orientation, regardless of tectonic province. Moderate damping divides Greenland between N–S (northern areas) and NE–SW (southern areas) fast orientations. However, these azimuths are continued well beyond the boundaries of the Greenland landmass, into the Arctic and North Atlantic oceans, respectively. Considerably more small-scale variation is observed in this study, both in the moderately smoothed maps shown and in more strongly smoothed versions of the tomographic inversion.

6 CONCLUSIONS

Using Rayleigh wave group velocities from regional earthquakes we have mapped out, for the first time, the 3-D anisotropic structure of the crust and uppermost mantle beneath Greenland and the western North Atlantic. The dense path coverage and broad period range allow us to examine lithospheric variations in unprecedented detail, shedding new light on the internal structure of a largely unexplored continental landmass. The Greenland crust is highly heterogeneous and anisotropic, reflecting the complex tectonic processes affecting the continent over its ∼4 Ga history.

The most significant sedimentary basins, such as the Danmarkshavn basin offshore NE Greenland, are clearly visible as regions of low shear wave velocity in the upper 10–15 km. Within the Greenland crust we observe significant lateral variations in shear wave velocity structure, with relatively low seismic velocities dominating to ∼25 km depth beneath northern Greenland, and generally higher velocities further to the south within the crust. The average crustal velocity is particularly high beneath central Greenland, and may be associated with a more mafic composition than the largely felsic crust elsewhere.

Crustal thickness, as inferred from velocity gradients and the transition to shear wave velocities over $\sim 4.2 \pm 0.2\,\mathrm{km\,s^{-1}}$, ranges from 25 km to almost 55 km beneath mainland Greenland. Offshore SE and central-E Greenland the crust thins significantly, with velocity profiles showing structures typical of rifted continental margins and the continent-ocean transition.

Uppermost-mantle velocity structure shows a clear distinction between the fast cratonic mantle beneath Greenland, including the continental-shelf region to the NE, and the slower mantle of the North Atlantic ocean basin. Seismic velocities in the oceanic mantle between Iceland and Greenland are particularly low, likely related to the effects of the Iceland hotspot. Beneath the Greenland mainland, we do not observe any pervasive modification of the upper-lithospheric mantle ($\leq$90 km depth) in the central region that is typically associated with the hotspot track. However, average crustal velocities are systematically higher in central Greenland than the northern or southern sections of the continent.

Patterns of azimuthal anisotropy are complex, particularly in the crust where amplitudes are generally high. Fast orientations in the crust vary on a scale of hundreds of km, consistent with the likely spatial variability of tectonic domains, and are generally best explained by large-scale alignments of anisotropic minerals, associated with metamorphic foliation and long-term crustal deformation.

ACKNOWLEDGEMENTS

FD acknowledges financial support from NSERC through their Discovery Grants and Canada Research Chairs programmes. Seismic waveform data were extracted from the IRIS DMS, the Geological Survey of Canada and the GEOFON (GFZ-Potsdam) archives (IPGP 1982; SIO 1986; ASL 1988; GEOFON 1993; Motyka *et al.* 2010; Lee 2013, GSC 2013). Winfried Hanka and John Clinton contributed valuable information on station timing and response. The GMT software package (Wessel & Smith 1998) was used for maps, graphs and interpolation of 1-D results for the pseudo-3-D model. Sergei Lebedev (Dublin Institute for Advanced Studies) provided the tomography codes, and Yingjie Yang, Juan Carlos Afonso and Zhen Guo (Macquarie University) provided the 1-D inversion codes for modelling the dispersion curves. We thank the Editor, reviewer Andrew Schaeffer and an anonymous reviewer for their helpful comments.

REFERENCES

Abbott, D.H., Mooney, W.D. & VanTongeren, J.A., 2013. The character of the Moho and lower crust within Archean cratons and the tectonic implications, *Tectonophysics,* **609,** 690–705.

Albuquerque Seismological Laboratory (ASL)/USGS, 1988. Global Seismograph Network (GSN - IRIS/USGS), International Federation of Digital Seismograph Networks. Other/Seismic Network, doi:10.7914/SN/IU.

Amante, C. & Eakins, B., 2009. *ETOPO1 Arc-Minute Global Relief Model: Procedures, Data Sources and Analysis*. Technical Report NGDC-24. NOAA Technical Memorandum NESDIS.

An, M. *et al.*, 2015. S-velocity model and inferred Moho topography beneath the Antarctic Plate from Rayleigh waves, *J. geophys. Res.,* **120,** 359–383.

Artemieva, I.M. & Thybo, H., 2013. EUNAseis: A seismic model for Moho and crustal structure in Europe, Greenland, and the North Atlantic region, *Tectonophysics,* **609,** 97–153.

Bamber, J.L., Layberry, R.L. & Gogineni, S., 2001. A new ice thickness and bed data set for the Greenland ice sheet: 1. Measurement, data reduction, and errors, *J. geophys. Res.,* **106,** 33 773–33 780.

Bensen, G., Ritzwoller, M. & Yang, Y., 2009. Shear velocity model of the crust and uppermost mantle beneath the United States from ambient seismic noise, *Geophys. J. Int.,* **177,** 1177–1196.

Braun, A., Kim, H.R., Csatho, B. & von Frese, R.R., 2007. Gravity-inferred crustal thickness of Greenland, *Earth planet. Sci. Lett.,* **262,** 138–158.

Brocher, T.M. & Christensen, N.I., 1990. Seismic anisotropy due to preferred mineral orientation observed in shallow crustal rocks in southern Alaska, *Geology,* **18,** 737–740.

Chalmers, J.A. & Pulvertaft, T., 2001. Development of the continental margins of the Labrador Sea: a review, *Geol. Soc. London Spec. Publ.,* **187,** 77–105.

Chian, D. & Louden, K., 1992. The structure of Archean-Ketilidian crust along the continental shelf of southwestern Greenland from a seismic refraction profile, *Can. J. Earth Sci.,* **29,** 301–313.

Chian, D. & Louden, K.E., 1994. The continent-ocean crustal transition across the southwest Greenland margin, *J. geophys. Res.,* **99,** 9117–9135.

Crampin, S., 1981. A review of wave motion in anisotropic and cracked elastic-media, *Wave Motion,* **3,** 343–391.

Crampin, S., 1994. The fracture criticality of crustal rocks, *Geophys. J. Int.,* **118,** 428–438.

Dahl-Jensen, T., Thybo, H., Hopper, J. & Rosing, M., 1998. Crustal structure at the SE Greenland margin from wide-angle and normal incidence seismic data, *Tectonophysics,* **288,** 191–198.

Dahl-Jensen, T. *et al.*, 2003. Depth to Moho in Greenland: receiver-function analysis suggests two Proterozoic blocks in Greenland, *Earth planet. Sci. Lett.,* **205,** 379–393.

Darbyshire, F.A., 2003. Crustal structure across the Canadian High Arctic region from teleseismic receiver function analysis, *Geophys. J. Int.,* **152,** 372–391.

Darbyshire, F.A., White, R.S. & Priestley, K.F., 2000. Structure of the crust and uppermost mantle of Iceland from a combined seismic and gravity study, *Earth planet. Sci. Lett.,* **181,** 409–428.

Darbyshire, F. *et al.*, 2004. A first detailed look at the Greenland lithosphere and upper mantle, using Rayleigh wave tomography, *Geophys. J. Int.,* **158,** 267–286.

Darbyshire, F. & Lebedev, S., 2009. Rayleigh wave phase-velocity heterogeneity and multilayered azimuthal anisotropy of the Superior Craton, Ontario, *Geophys. J. Int.,* **176,** 215–234.

Darbyshire, F.A., Eaton, D.W. & Bastow, I.D., 2013. Seismic imaging of the lithosphere beneath Hudson Bay: episodic growth of the Laurentian mantle keel, *Earth planet. Sci. Lett.,* **373,** 179–193.

Darbyshire, F., Bastow, I., Petrescu, L., Gilligan, A. & Thompson, D., 2017. A tale of two orogens: crustal processes in the Proterozoic Trans-Hudson and Grenville Orogens, eastern Canada, *Tectonics,* **36,** doi:10.1002/2017TC004479.

Dawes, P.R., 2009. The bedrock geology under the Inland Ice: the next major challenge for Greenland mapping, *Geol. Surv. Denmark Greenland Bull.,* **17,** 57–60.

Deschamps, F., Lebedev, S., Meier, T. & Trampert, J., 2008. Azimuthal anisotropy of Rayleigh-wave phase velocities in the east-central US, *Geophys. J. Int.,* **173,** 827–843.

Dick, H.J., Lin, J. & Schouten, H., 2003. An ultraslow-spreading class of ocean ridge, *Nature,* **426,** 405–412.

Døssing, A., Dahl-Jensen, T., Thybo, H., Mjelde, R. & Nishimura, Y., 2008. East Greenland Ridge in the North Atlantic Ocean: An integrated geophysical study of a continental sliver in a boundary transform fault setting, *J. geophys. Res.,* **113,** B10107, doi:10.1029/2007JB005536.

Durrheim, R. & Mooney, W., 1991. Archean and Proterozoic Crustal Evolution: Evidence from Crustal Seismology, *Geology,* **19,** 606—609.

Dziewonski, A. & Anderson, D., 1981. Preliminary reference Earth model, *Phys. Earth planet. Inter.,* **25,** 297–356.

GSC, 2013–2014. Earthquakes Canada, Continuous Waveform Archive, *Nat. Res. Can.,* http://earthquakescanada.nrcan.gc.ca/stndon/AutoDRM/index-eng.php.

Engen, Ø., Faleide, J.I. & Dyreng, T.K., 2008. Opening of the Fram Strait gateway: a review of plate tectonic constraints, *Tectonophysics,* **450,** 51–69.

Fechner, N. & Jokat, W., 1996. Seismic refraction investigations on the crustal structure of the western Jameson Land Basin, East Greenland, *J. geophys. Res.,* **101,** 15 867–15 881.

Funck, T., Jackson, H.R., Dehler, S.A. & Reid, I.D., 2006. A refraction seismic transect from Greenland to Ellesmere island, Canada: the crustal structure in southern Nares Strait, *Polarforschung,* **74,** 97–112.

Funck, T., Jackson, H.R., Louden, K.E. & Klingelhöfer, F., 2007. Seismic study of the transform-rifted margin in Davis Strait between Baffin Island (Canada) and Greenland: What happens when a plume meets a transform, *J. geophys. Res.,* **112,** B04402, doi:10.1029/2006JB004308.

Funck, T., Gohl, K., Damm, V. & Heyde, I., 2012. Tectonic evolution of southern Baffin Bay and Davis Strait: results from a seismic refraction transect between Canada and Greenland, *J. geophys. Res.,* **117,** B04107, doi:10.1029/2011JB009110.

Gaina, C., Medvedev, S., Torsvik, T.H., Koulakov, I. & Werner, S.C., 2014. 4D Arctic: a glimpse into the structure and evolution of the Arctic in the light of new geophysical maps, plate tectonics and tomographic models, *Surv. Geophys.,* **35,** 1095–1122.

GEOFON Data Centre, 1993. GEOFON Seismic Network, Deutsches GeoForschungsZentrum GFZ, doi:10.14470/tr560404.

Gerlings, J., Funck, T., Jackson, H.R., Louden, K.E. & Klingelhöfer, F., 2009. Seismic evidence for plume-derived volcanism during formation of the continental margin in southern Davis Strait and northern Labrador Sea, *Geophys. J. Int.,* **176,** 980–994.

Gohl, K. & Smithson, S.B., 1993. Structure of Archean crust and passive margin of southwest Greenland from seismic wide-angle data, *J. geophys. Res.,* **98,** 6623–6638.

Gregersen, S., 1970. Surface wave dispersion and crust structure in Greenland, *Geophy. J. R. astr. Soc.,* **22,** 29–39.

Guo, Z. *et al.*, 2015. High resolution 3-D crustal structure beneath NE China from joint inversion of ambient noise and receiver functions using NECESSArray data, *Earth planet. Sci. Lett.,* **416,** doi:10.1016/j.epsl.2015.01.044.

Guo, Z., Chen, Y.J., Ning, J., Yang, Y., Afonso, J.C. & Tang, Y., 2016. Seismic evidence of on-going sublithosphere upper mantle convection for intra-plate volcanism in Northeast China, *Earth planet. Sci. Lett.,* **433,** 31–43.

Haario, H., Laine, M., Mira, A. & Saksman, E., 2006. DRAM: efficient adaptive MCMC, *Stat. Comput.,* **16,** 339–354.

Henriksen, N., Higgins, A., Kalsbeek, F. & Pulvertaft, T.C.R., 2009. Greenland from Archaean to Quaternary: descriptive text to the 1995 geological map of Greenland, 1: 2 500 000, 2nd edn, Geol. Surv. Denmark Greenland Bull., **18,** 126 pp.

Hermann, T. & Jokat, W., 2013. Crustal structures of the Boreas Basin and the Knipovich Ridge, North Atlantic, *Geophys. J. Int.,* **193,** 1399–1414.

Herrmann, R.B., 2013. Computer programs in seismology: an evolving tool for instruction and research, *Seismol. Res. Lett.,* **84,** 1081–1088.

Holbrook, W.S. *et al.*, 2001. Mantle thermal structure and active upwelling during continental breakup in the North Atlantic, *Earth planet. Sci. Lett.,* **190,** 251–266.

Hopper, J.R., Dahl-Jensen, T., Holbrook, W.S., Larsen, H.C., Lizarralde, D., Korenaga, J., Kent, G.M. & Kelemen, P.B., 2003. Structure of the SE Greenland margin from seismic reflection and refraction data: implications for nascent spreading center subsidence and asymmetric crustal accretion during North Atlantic opening, *J. geophys. Res.,* **108,** 2269, doi:10.1029/2002JB001996.

Institut De Physique Du Globe De Paris & Ecole Et Observatoire Des Sciences De La Terre De Strasbourg, 1982. GEOSCOPE, French Global Network of broad band seismic stations. Institut de Physique du Globe de Paris (IPGP), doi:10.18715/geoscope.g.

Jackson, H.R. & Dahl-Jensen, T., 2010. Sedimentary and crustal structure from the Ellesmere Island and Greenland continental shelves onto the Lomonosov Ridge, Arctic Ocean, *Geophys. J. Int.,* **182,** 11–35.

Jackson, H.R. & Reid, I., 1994. Crustal thickness variations between the Greenland and Ellesmere Island margins determined from seismic refraction, *Can. J. Earth Sci.,* **31,** 1407–1418.

Jackson, H.R., Johnson, G.L., Sundvor, E. & Myhre, A.M., 1984. The Yermak Plateau: Formed at a triple junction, *J. geophys. Res.,* **89,** 3223–3232.

Jakovlev, A., Bushenkova, N., Koulakov, I.Y. & Dobretsov, N., 2012. Structure of the upper mantle in the Circum-Arctic region from regional seismic tomography, *Russ. Geol. Geophys.,* **53,** 963–971.

Kao, H. *et al.*, 2013. Ambient seismic noise tomography of Canada and adjacent regions: Part I. Crustal structures, *J. geophys. Res.,* **118,** 5865–5887.

Kennett, B., Engdahl, E. & Buland, R., 1995. Constraints on seismic velocities in the earth from travel times, *Geophys. J. Int.,* **122,** 108–124.

Kodaira, S., Mjelde, R., Gunnarsson, K., Shiobara, H. & Shimamura, H., 1997. Crustal structure of the Kolbeinsey Ridge, North Atlantic, obtained by use of ocean bottom seismographs, *J. geophys. Res.,* **102,** 3131–3151.

Korenaga, J., Holbrook, W., Kent, G., Kelemen, P., Detrick, R., Larsen, H.C., Hopper, J. & Dahl-Jensen, T., 2000. Crustal structure of the southeast Greenland margin from joint refraction and reflection seismic tomography, *J. geophys. Res.,* **105,** 21 591–21 614.

Kumar, P., Kind, R., Priestley, K. & Dahl-Jensen, T., 2007. Crustal structure of Iceland and Greenland from receiver function studies, *J. geophys. Res.,* **112,** B03301, doi:10.1029/2005JB003991.

Laske, G., Masters, G., Ma, Z. & Pasyanos, M., 2013. Update on CRUST1.0 - a 1-degree global model of Earth's crust, *Geophys. Res. Abstr.,* **15,** EGU2013–2658.

Laske, G. & Masters, G., 1997. A global digital map of sediment thickness, *EOS, Trans. Am. geophys. Un.,* **78,** F483.

Lebedev, S., Boonen, J. & Trampert, J., 2009. Seismic structure of Precambrian lithosphere: new constraints from broad-band surface-wave dispersion, *Lithos,* **109,** 96–111.

Lebedev, S., Adam, J.M.C. & Meier, T., 2013. Mapping the Moho with seismic surface waves: a review, resolution analysis, and recommended inversion strategies, *Tectonophysics,* **609,** 377–394.

Lebedev, S., Schaeffer, A.J., Fullea, J. & Pease, V., 2017. Seismic tomography of the Arctic region: inferences for the thermal structure and evolution of the lithosphere, *Geol. Soc. London Spec. Publ.,* **460,** SP460–10. doi:10.1144/SP460.10.

Lee, W.S., 2013. Korea Polar Observation Network. International Federation of Digital Seismograph Networks. Other/Seismic Network, doi:10.7914/SN/KP.

Levshin, A., Ratnikova, L. & Berger, J., 1992. Peculiarities of surface-wave propagation across central Eurasia, *Bull. seism. Soc. Am.,* **82,** 2464–2493.

Levshin, A., Ritzwoller, M., Barmin, M., Villasenor, A. & Padgett, C., 2001. New constraints on the arctic crust and uppermost mantle: surface wave group velocities, Pn, and Sn, *Phys. Earth planet. Inter.,* **123,** 185–204.

Lin, F.C. & Schmandt, B., 2014. Upper crustal azimuthal anisotropy across the contiguous US determined by Rayleigh wave ellipticity, *Geophys. Res. Lett.,* **41,** 8301–8307.

Lin, F.C., Ritzwoller, M.H., Yang, Y., Moschetti, M.P. & Fouch, M.J., 2011. Complex and variable crustal and uppermost mantle seismic anisotropy in the western United States, *Nat. Geosci.,* **4,** 55–61.

Masters, G., Barmine, M. & Kientz, S., 2007. *Mineos User's Manual in Computational Infrastructure for Geodynamics,* California Institute of Technology, pp. 1–97.

Meltzer, A. & Christensen, N., 2001. Nanga Parbat crustal anisotropy: implications for interpretation of crustal velocity structure and shear wave splitting, *Geophys. Res. Lett.,* **28,** 2129–2132.

Mosegaard, K. & Tarantola, A., 1995. Monte Carlo sampling of solutions to inverse problems, *J. geophys. Res.,* **100,** 12 431–12 447.

Motyka, R., Fahnestock, M. & Truffer, M., 2010. Ice-ocean interaction at Nuuk tidewater glaciers. International Federation of Digital Seismograph Networks. Other/Seismic Network, doi:10.7914/SN/9D_2010.

Nielsen, T.K., Larsen, H.C. & Hopper, J.R., 2002. Contrasting rifted margin styles south of Greenland: implications for mantle plume dynamics, *Earth planet. Sci. Lett.,* **200,** 271–286.

Nutman, A.P., Dawes, P.R., Kalsbeek, F. & Hamilton, M.A., 2008. Palaeoproterozoic and Archaean gneiss complexes in northern Greenland: palaeoproterozoic terrane assembly in the High Arctic, *Precambrian Res.,* **161,** 419–451.

Paige, C. & Saunders, M., 1982. LSQR: An algorithm for sparse linear equations and sparse least squares, *Assoc. Comput. Mach. Trans. Math. Softw.* **8,** 43–71.

Pawlak, A., Eaton, D., Darbyshire, F., Lebedev, S. & Bastow, I., 2012. Crustal anisotropy beneath Hudson Bay from ambient-noise tomography: evidence for post-orogenic lower-crustal flow?, *J. geophys. Res.,* **117,** B08301, doi:10.1029/2011JB009066.

Peters, L., Anandakrishnan, S., Alley, R. & Voigt, D., 2012. Seismic attenuation in glacial ice: a proxy for englacial temperature, *J. geophys. Res.,* **117,** F02008, doi:10.1029/2011JF002201.

Petrescu, L., Bastow, I., Darbyshire, F., Gilligan, A., Bodin, T., Menke, W. & Levin, V., 2016. Three billion years of crustal evolution in eastern Canada: constraints from receiver functions, *J. geophys. Res.,* **121,** 788–811.

Petrov, O. *et al.*, 2016. Crustal structure and tectonic model of the Arctic region, *Earth Sci. Rev.,* **154,** 29–71.

Pilidou, S., Priestley, K., Gudmundsson, O. & Debayle, E., 2004. Upper mantle S-wave speed heterogeneity and anisotropy beneath the North Atlantic from regional surface wave tomography: The Iceland and Azores plumes, *Geophys. J. Int.,* **159,** 1057–1076.

Pilidou, S., Priestley, K., Debayle, E. & Gudmundsson, O., 2005. Rayleigh wave tomography in the North Atlantic: high resolution images of the Iceland, Azores and Eifel mantle plumes, *Lithos,* **79,** 453–474.

Reid, I. & Jackson, H., 1997. Crustal structure of northern Baffin Bay: seismic refraction results and tectonic implications, *J. geophys. Res.,* **102,** 523–542.

Rickers, F., Fichtner, A. & Trampert, J., 2013. The Iceland–Jan Mayen plume system and its impact on mantle dynamics in the North Atlantic region: evidence from full-waveform inversion, *Earth planet. Sci. Lett.,* **367,** 39–51.

Ritsema, J., Deuss, A., van Heijst, H. & Woodhouse, J., 2011. S40RTS: a degree-40 shear-velocity model for the mantle from new Rayleigh wave dispersion, teleseismic traveltime and normal-mode splitting function measurements, *Geophys. J. Int.,* **184,** 1223–1236.

Ritzmann, O. & Jokat, W., 2003. Crustal structure of northwestern Svalbard and the adjacent Yermak Plateau: evidence for Oligocene detachment tectonics and non-volcanic breakup, *Geophys. J. Int.,* **152,** 139–159.

Ritzmann, O., Jokat, W., Czuba, W., Guterch, A., Mjelde, R. & Nishimura, Y., 2004. A deep seismic transect from Hovgård Ridge to northwestern Svalbard across the continental-ocean transition: a sheared margin study, *Geophys. J. Int.,* **157,** 683–702.

Rogozhina, I. *et al.*, 2016. Melting at the base of the Greenland ice sheet explained by Iceland hotspot history, *Nat. Geosci.,* **9,** 366–369.

Salmon, M., Kennett, B. & Saygin, E., 2013. Australian seismological reference model (AuSREM): crustal component, *Geophys. J. Int.,* **192,** 190–206.

Schaeffer, A. & Lebedev, S., 2013. Global shear speed structure of the upper mantle and transition zone, *Geophys. J. Int.,* **194,** 417–449.

Schaeffer, A. & Lebedev, S., 2014. Imaging the North American continent using waveform inversion of global and USArray data, *Earth planet. Sci. Lett.,* **402,** 26–41.

Schaeffer, A., Lebedev, S. & Becker, T., 2016. Azimuthal seismic anisotropy in the Earth's upper mantle and the thickness of tectonic plates, *Geophys. J. Int.,* **207,** 901–933.

Schiffer, C., Balling, N., Jacobsen, B.H., Stephenson, R.A. & Nielsen, S.B., 2014. Seismological evidence for a fossil subduction zone in the East Greenland Caledonides, *Geology,* **42,** 311–314.

Schlindwein, V. & Jokat, W., 1999. Structure and evolution of the continental crust of northern east Greenland from integrated geophysical studies, *J. geophys. Res.,* **104,** 15 227–15 245.

Schmidt-Aursch, M.C. & Jokat, W., 2005. The crustal structure of central East Greenland: from the Caledonian orogen to the Tertiary igneous province, *Geophys. J. Int.,* **160,** 736–752.

Scripps Institution of Oceanography (SIO), 1986. IRIS/IDA Seismic Network. International Federation of Digital Seismograph Networks. Other/Seismic Network, doi:10.7914/SN/II.

Shen, W. & Ritzwoller, M.H., 2016. Crustal and uppermost mantle structure beneath the United States, *J. geophys. Res.,* **121,** 4306–4342.

Shen, W. *et al.*, 2016. A seismic reference model for the crust and uppermost mantle beneath China from surface wave dispersion, *Geophys. J. Int.,* **206,** 954–979.

Silver, P.G. & Chan, W.W., 1991. Shear wave splitting and subcontinental mantle deformation, *J. geophys. Res.,* **96,** 16 429–16 454.

Singh, A., Singh, C. & Kennett, B., 2015. A review of crust and upper mantle structure beneath the Indian subcontinent, *Tectonophysics,* **644,** 1–21.

Sleep, N., 1997. Lateral flow and ponding of starting plume material, *J. geophys. Res.,* **102,** 10 001–10 012.

Sleep, N., 2003. Survival of Archean cratonal lithosphere, *J. geophys. Res.,* **108,** 2302, doi:10.1029/2001JB000169.

Smallwood, J.R., Staples, R.K., Richardson, K.R. & White, R.S., 1999. Crust generated above the Iceland mantle plume: from continental rift to oceanic spreading center, *J. geophys. Res.,* **104,** 22 885–22 902.

Smith, M. & Dahlen, F., 1973. The azimuthal dependence of Love and Rayleigh wave propagation in a slightly anisotropic medium, *J. geophys. Res.,* **78,** 3321–3333.

Steffen, R., Strykowski, G. & Lund, B., 2017. High-resolution Moho model for Greenland from EIGEN-6C4 gravity data, *Tectonophysics,* **706,** 206–220.

St-Onge, M.R., Van Gool, J.A., Garde, A.A. & Scott, D.J., 2009. Correlation of Archaean and Palaeoproterozoic units between northeastern Canada

and western Greenland: constraining the pre-collisional upper plate accretionary history of the Trans-Hudson orogen, *Geol. Soc. London Spec. Publ.,* **318,** 193–235.

Suckro, S.K. *et al.*, 2012. The crustal structure of southern Baffin Bay: implications from a seismic refraction experiment, *Geophys. J. Int.,* **190,** 37–58.

Suckro, S.K., Gohl, K., Funck, T., Heyde, I., Schreckenberger, B., Gerlings, J. & Damm, V., 2013. The Davis Strait crust: a transform margin between two oceanic basins, *Geophys. J. Int.,* **193,** 78–97.

Talwani, M. & Eldholm, O., 1977. Evolution of the Norwegian-Greenland sea, *Geol. soc. Am. Bull.,* **88,** 969–999.

Tarantola, A., 2005. *Inverse Problem Theory and Methods for Model Parameter Estimation,* SIAM.

Torsvik, T.H., Carlos, D., Mosar, J., Cocks, L.R.M. & Malme, T.N., 2002. Global reconstructions and North Atlantic paleogeography 440 Ma to recent, in *BATLAS—Mid Norway Plate Reconstruction Atlas with Global and Atlantic Perspectives,* pp. 18–39, ed. Eide, E.A., Geological Survey of Norway.

van Gool, J.A., Connelly, J.N., Marker, M. & Mengel, F.C., 2002. The Nagssugtoqidian Orogen of West Greenland: tectonic evolution and regional correlations from a West Greenland perspective, *Can. J. Earth Sci.,* **39,** 665–686.

Verhoef, J., Roest, W.R., Macnab, R., Arkani-Hamed, J. & Project Team, 1996. Magnetic anomalies of the Arctic and North Atlantic oceans and adjacent land areas, Geol. Surv. Can. Open File 3125.

Voss, M. & Jokat, W., 2007. Continent–ocean transition and voluminous magmatic underplating derived from *P*-wave velocity modelling of the East Greenland continental margin, *Geophys. J. Int.,* **170,** 580–604.

Voss, M., Schmidt-Aursch, M.C. & Jokat, W., 2009. Variations in magmatic processes along the East Greenland volcanic margin, *Geophys. J. Int.,* **177,** 755–782.

Weigel, W. *et al.*, 1995. Investigations of the East Greenland continental margin between 70 and 72 N by deep seismic sounding and gravity studies, *Mar. Geophys. Res.,* **17,** 167–199.

Wessel, P. & Smith, W., 1998. New, improved version of Generic Mapping Tools released, *EOS, Trans. Am. geophys. Un.,* **79,** 579.

Yao, H., van der Hilst, R.D. & Montagner, J.P., 2010. Heterogeneity and anisotropy of the lithosphere of SE Tibet from surface wave array tomography, *J. geophys. Res.,* **115,** B12307, doi:10.1029/2009JB007142.

SUPPORTING INFORMATION

Supplementary data are available at *GJI* online.

Figure S1. Moho depths from previous seismic studies.
Figure S2. Resolution tests for leakage between isotropic and anisotropic components at 25 s period.
Figure S3. Resolution tests at 50 and 75 s period.
Figure S4. Histograms for anisotropic parameters.
Figure S5. Group velocity maps for remaining periods 15–75 s.
Figure S6. Effect of ray width on group velocity maps.
Figure S7. Examples of 1-D modelling of dispersion curves.
Figure S8. Examples of 1-D modelling of dispersion curves *(continued)*.
Figure S9. Examples of 1-D modelling of dispersion curves *(continued)*.
Table S1. Worst-case values for leakage between isotropic and anisotropic parameters in ‘checkerboard’ and ‘structural’ resolution tests at 25, 50 and 70 s period.
Table S2. Model statistics for the dispersion curves shown in Figs S7–S9.

Please note: Oxford University Press is not responsible for the content or functionality of any supporting materials supplied by the authors. Any queries (other than missing material) should be directed to the corresponding author for the paper.